Method to deterministically generate large-amplitude optical cat states

Check for updates

Zheng-Hong Li [1,2,6] ✉, Fei Yu[1], Zhen-Ya Li[1], M. Al-Amri [3,4,5,6] ✉ & M. Suhail Zubairy [3,6] ✉

Cat states, as an important resource in the study of macroscopic quantum superposition and quantum information applications, have garnered widespread attention. To date, preparing large-sized optical cat states has remained challenging. We demonstrate that, by utilizing interaction-free measurement and the quantum Zeno effect, even a fragile quantum microscopic system can deterministically control and become entangled with strong light fields, thereby generating large-amplitude optical cat states. During the entire preparation process, our method ensures that the microscopic system functions within a weak field environment, so that its quantum property can be protected. Furthermore, we show that the preparation of cat states is possible even when the quantum microsystem suffers from significant photon loss, provided that optical losses from classical devices are kept low, which implies that the fidelity of the cat state can be enhanced by improvements to and the perfection of the classical optical system.

Schrödinger's gedanken experiment involving a cat in a superposition of dead and alive states vividly demonstrates the magical picture of quantum superposition on a macro scale[1]. In modern physics, this cat state (CS) is usually represented by the superposition of two distinct coherent states $|\pm\alpha\rangle$, which can generally be considered orthogonal when $|\alpha| \geq 2$. With the increase of amplitude $|\alpha|$, CS gets closer to the macroscopic superposition, making it an important resource for the study of macroscopic quantum phenomena. CS is not only attractive from a fundamental point of view[2,3], but also valuable for applications including quantum teleportation[4-6], quantum computing[7-11], quantum error correction[12-17] and quantum metrology[18-24]. After decades of efforts, CS is now being generated on various platforms[3,25-28]. However, even for the best experimental results in the optical domain so far $|\alpha|$ remains less than 2[29-37], and it remains a challenge to increase the value of $|\alpha|$ based on existing methods. For example, the widely studied photon subtraction method[29-33,38,39], which is a probabilistic method based on post-selection, has low probability of success for generating large-amplitude CS. Another approach that has attracted a lot of attention is the synthesis method[36,40,41], which uses a pre-prepared CS as a seed to grow large-amplitude CS. However, this method is still limited by the amplitude of the pre-prepared CS. Furthermore, a deterministic method that based on light-matter interaction[42] has recently been demonstrated experimentally[37]. In this method, CS is generated by direct interaction between an incident coherent light pulse and a single-side cavity containing a three-level atom[37,42-45]. Its basic idea is to use normal-mode splitting[43] to control the phase of the reflected coherent light field. In the experiment, the amplitude of the output CS is $|\alpha| \approx 1.4$[37]. Unfortunately, this method is limited in preparing an arbitrarily large $|\alpha|$ CS for a given optical pulse length, due to the fragility of the atom-cavity coupling system when interacting with a strong light field. As the external field strengthens, a single atom ultimately cannot prevent the optical field from entering the cavity, resulting in the reflected field carrying a π phase shift regardless of the atomic state, similar to what occurs with empty cavity reflection.

Needless to say, optical field is an excellent medium for information transmission. Considering the practical application requirements that involve integrating diverse quantum systems, as well as for advanced sensing and imaging techniques, the generation of optical CS with large amplitudes and customizable propagation properties becomes not only necessary but also of significant value. This endeavor represents a pioneering frontier in the realm of quantum optics, bearing profound implications for both the theoretical understanding and the advancement of practical quantum technology[46].

In this article, we propose a deterministic method to generate flying optical CS whose amplitude can be arbitrarily large, provided that optical losses from classical optical devices remain low. The key step of our scheme

[1]Institute for Quantum Science and Technology and Department of Physics, Shanghai University, Shanghai 200444, China. [2]Shanghai Key Laboratory of High Temperature Superconductors, Shanghai University, Shanghai 200444, China. [3]Institute for Quantum Science and Engineering (IQSE) and Department of Physics and Astronomy, Texas A&M University, College Station, Texas, TX 77843-4242, USA. [4]NCQOQI, KACST, P.O.Box 6086, Riyadh 11442, Saudi Arabia. [5]Institute of Quantum Technologies and Advanced Computing, KACST, Riyadh 11442, Saudi Arabia. [6]These authors contributed equally: Zheng-Hong Li, M. Al-Amri, M. Suhail Zubairy. ✉e-mail: refirefox@shu.edu.cn; mdalamri@kacst.gov.sa; zubairy@physics.tamu.edu
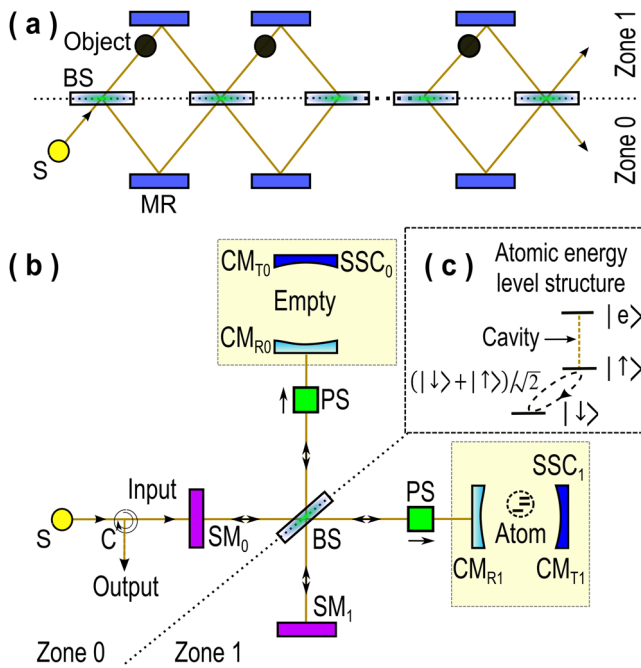
1

Fig. 1 | Schematic for cat state preparation. S represents the coherent light source, BS the beam-splitter, MR the normal mirror, SM the switchable mirror, PS the phase shifter, and C the optical circulator. **a** Principle model based on a chain interferometer. **b** Multiple reflection scheme based on a Michelson interferometer. When the switchable mirrors (SM) are turned on, the coherent light pulse bounces inside the interferometer and interacts with the single-side cavity (SSC) M times. The SSC consists of two mirrors, CM_T and CM_R, with CM_T assumed to have perfect reflectivity under ideal conditions. Only SSC_1 contains a three-level atom. **c** The energy level structure of the atom, where the cavity mode couples only with the transition between levels $|\uparrow\rangle$ and $|e\rangle$. The atom is prepared in superposition state $(|\downarrow\rangle + |\uparrow\rangle)/\sqrt{2}$.

is to entangle a strong coherent light field with a microscopic quantum system prepared in a superposition state initially. After the entanglement, the optical CS is obtained by performing projection measurement on the quantum microsystem. In response to the situation that a quantum microsystem is typically very fragile when facing strong light fields, our solution is to utilize interaction-free measurement based on quantum Zeno effect[47–49], which is considered a powerful non-invasive measurement method that can protect vulnerable samples. In this work, we further apply it to protect the quantum properties of the microscopic system from destruction by strong fields. We replace the direct interaction between the strong light field and the microsystem with a sequence of interactions, each with only a small fraction of photons actually interacting with the microsystem. This ensures that the quantum microsystem always works in a weak field environment, making one of the main advantages of this work. Eliminating the negative influence of strong fields gives liberty of applying this method in a wide variety of systems and provides the potential for future applications. More importantly, this indicates that our scheme allows quantum microscopic systems to manipulate macroscopic counterparts that are challenging to control directly. In addition, our method has another important advantage—it can reduce the requirements of quantum microscopic systems. For illustration, we employ the single-side cavity-atom coupling model[37] as our specific quantum microscopic system. Our simulation shows that our scheme becomes less and less sensitive to both atomic spontaneous emission and detuning between the atom and the cavity as the number of interactions increases, when other classical optical devices are ideal. This enables our method to reduce the impact of optical losses originating from quantum device (referred to as Type I light loss), with the main limitation of our method arising from the optical losses introduced by classical optical devices (referred to as Type II light loss).

worth mentioning that here we mainly focus on the optical platform, but our approach can also be extended to other platforms such as superconducting microwave resonator[50,51].

Results and discussion
General multiple reflection scheme

First, we focus on explaining the principle of our method. More detailed experimental protocols will be discussed later. We start with the chain Mach-Zehnder interferometer shown in Fig. 1a, which is a commonly used optical structure for interaction-free measurement[52–57]. Compared to conventional interaction-free measurement studies, our scheme has two distinct features, although these are commonly used and even necessary for CS preparation. Firstly, we use a coherent light source (S) instead of a single photon source. Secondly, conventional interaction-free measurement typically assume that an object has two functions: absorbing photons or allowing them to pass through. However, our method introduces an additional function for the object, which is to apply a π phase shift to the light field passing through it. In details, as shown in Fig. 1a, MR stands for normal mirror, and BS stands for beam-splitter. The interference occurs between the light fields in Zones 0 and 1, which are located on the lower and upper sides of BS, respectively, separated by a dotted line. Assuming that $a_z^\dagger$ ($z = 0, 1$) represents the creation operator of the light field in Zone z, the function of BS can be described by $a_0^\dagger \rightarrow a_0^\dagger \cos\theta + a_1^\dagger \sin\theta$ and $a_1^\dagger \rightarrow a_1^\dagger \cos\theta - a_0^\dagger \sin\theta$[49], where $\cos^2\theta$ represents the reflectivity of BS. As for the object, it has three states, $|pass\rangle$, $|block\rangle$, and $|phase\rangle$. Firstly, we discuss the state $|pass\rangle$, where the object is transparent, thereby causing optical interference to occur continuously in Zones 0 and 1. Assuming the initial state of the light field is such that the field in Zone 0 is in the coherent state $|\alpha\rangle$ and the field in Zone 1 is in the vacuum state $|0\rangle$, it is represented as $|\alpha, 0\rangle = \exp(\alpha a_0^\dagger - \alpha^* a_0)|0, 0\rangle$. After passing through N number of BSs, it becomes $|\alpha\cos N\theta, \alpha\sin N\theta\rangle$[58]. Apparently, when $\theta = \pi/2N$, we have $|0, \alpha\rangle$. While when $\theta = \pi/N$, we have $|-\alpha, 0\rangle$. Secondly, we discuss the state $|block\rangle$. In this case, any photon passing through the object is absorbed. Notice that the object and the light field interact many times. To take into account all absorbed photons, we write the state of the light field as $|C_0, C_1\rangle|l_1, l_2, \ldots l_{N-1}\rangle$, where $|C_{z=0,1}\rangle$ represents photon state in Zone z and $|l_1, l_2, \ldots l_{N-1}\rangle$ represents the photon absorbed each time. After the light pulse passing through the first BS, the initial state $|\alpha, 0\rangle|0, 0, \ldots 0\rangle$ evolves to $|\alpha\cos\theta, \alpha\sin\theta\rangle|0, 0, \ldots 0\rangle$, and it further becomes $|\alpha\cos\theta, 0\rangle|\alpha\sin\theta, 0, \ldots 0\rangle$ due to the absorption of the object. Subsequently, the photons remaining inside the interferometers pass through the next BS and interact with the object again. Such process repeats N times. After N numbers of BSs, the photon state is $|\alpha\cos^N\theta, \alpha\cos^{N-1}\theta\sin\theta\rangle \prod_{n=1}^{N-1}|\alpha\cos^{n-1}\theta\sin\theta\rangle$. Note that when $\theta = \pi/N$, as $N \rightarrow \infty$, we have $\cos^N\theta \rightarrow 1$ and $\sin\theta \rightarrow 0$. Therefore, as long as $|\alpha|^2$ is finite, the light field can be frozen in its initial state $|\alpha, 0\rangle|0, 0, \ldots 0\rangle$. This also means that the actual number of photons absorbed by the object during the entire process is close to zero. The object is spared from being directly exposed to light field due to the interruption of the interference process, which can be considered the quantum Zeno effect caused by photon loss. Besides the state $|block\rangle$, the state $|phase\rangle$ can also maintain the light field in its initial state by applying a π phase shift ($a_1^\dagger \rightarrow -a_1^\dagger$) to the photons passing through it. When the photons encounter an odd number of BS, the state becomes $|\alpha\cos\theta, \alpha\sin\theta\rangle$, while after passing through an even number of BS, it becomes $|\alpha, 0\rangle$. It's important to note that the maximum intensity of photons actually passing through the object during each interaction is $|\alpha\sin\theta|^2$. When $\theta = \pi/N$, this value tends to zero as N increases, suggesting the freezing of the light field. Consequently, for both states $|block\rangle$ and $|phase\rangle$, the object works in a weak field environment.

Above, we have introduced the three states of the object and the corresponding dynamic evolution behavior of the light field. It is easy to see that if an object is initially in a superposition state of $(|pass\rangle + |block\rangle)/\sqrt{2}$ or $(|pass\rangle + |phase\rangle)/\sqrt{2}$, the object can be entangled with the coherent light field when $\theta = \pi/N$, i.e., $(|-\alpha, 0\rangle|pass\rangle + |\alpha, 0\rangle|block/phase\rangle)/\sqrt{2}$. After measuring the object with $(|pass\rangle \pm |block/phase\rangle)/\sqrt{2}$, CS can be deterministically created. However, whether it turns out to be an odd or even

Article

CS is random, each with a 50% probability of occurrence. The even CS occurs when the measurement result is $(|\text{pass}\rangle + |\text{block/phase}\rangle)/\sqrt{2}$. As for the other measurement result, the odd CS is obtained. In addition, it is worth mentioning that our method can also realize the entangled coherent state $(|\alpha, 0\rangle + |0, \alpha\rangle)/\sqrt{2}$[20,21]. To do so, we just need to set $\theta = \pi/2N$. Given that the optical field is reflected and interacts with the quantum object many times, we refer to the above method as the multiple reflection scheme in the following discussion.

Multiple reflection scheme using single-side cavity-atom coupling system

The above is the basic idea of our method. The next important issue is what kind of real quantum microscopic system can be used as an object for our scheme. We have shown that it is optional whether the object absorbs photons or provides a π phase. The difference is that the latter way does not introduce any photon loss. In theory, it has better fidelity. Nevertheless, given that photon loss due to device imperfection is inevitable in real systems, the former mechanism is also critical. In fact, our later numerical calculations will show that such mechanism can even mitigate the impact of optical losses caused by the quantum system, indicating that the optical loss of the quantum microsystem no longer serves as the decisive factor when choosing a microsystem for our multiple reflection scheme. Microsystems capable of implementing optical path blocking, such as Rydberg blockade[59–61], photon blockade[62], and so on[58,63], remain viable candidates for applying our method. Regardless of the system type, our scheme allows the microsystem to function properly within a weak field environment. This represents the primary contribution of our work, enabling our scheme to be utilized in any given experimental environment and offering potential for future practical application. In the following, we will analyze a detailed experimental scheme based on a specific microscopic system in order to study the performance of our method under realistic conditions.

For illustrative purposes only, we adopt the atom-single side cavity system[37] as our quantum microsystem. As shown in Fig. 1b, a single atom is embedded in a single-side cavity SSC$_1$, which is constituted by two facing mirrors CM$_R$ and CM$_T$. Ideally, CM$_T$ is assumed to have perfect reflection, but CM$_R$ is allowed for in- and outcoupling of light. The energy level configuration of the atom is shown in Fig. 1c. The transition between levels $|\uparrow\rangle$ and $|e\rangle$ is coupled by the cavity mode. When the atom is in $|\uparrow\rangle$, the weak coherent light pulse, resonant with the cavity, is prevented from entering the cavity due to normal-mode splitting, which results in reflection without a π phase shift. As for the transition between $|\downarrow\rangle$ and $|\uparrow\rangle$, it is decoupled from the cavity mode due to large detuning. Therefore, when the atom is in $|\downarrow\rangle$, the cavity can be treated as an empty cavity. The incident pulse enters the cavity and reflects back but with a π phase. This atom-cavity coupling model has been directly used to generate CS[37,42]. After a single reflection (Hereinafter we call it the single reflection scheme), the atom-field entanglement $(|\alpha\rangle|\uparrow\rangle + |-\alpha\rangle|\downarrow\rangle)/\sqrt{2}$ can be generated. Unfortunately, we will later explain why the method becomes ineffective when the incident light field is strong, but our solution can address this problem.

Based on the atom-cavity system, our detailed experimental scheme is presented in Fig. 1b. In order to implement multiple interactions between the atom and light field, we do not directly use the chain interferometer structure in Fig. 1a, but rather its equivalent Michelson interferometer. In the figure, SM stands for switchable mirror (In the experiment, it can be realized by a fiber switch[64] or Pockels cell[65–68]), which is transparent only at the beginning and end of preparation. At all other times, it is just a normal mirror, forcing the light pulse to bounce back and forth inside the interferometer for M cycles. One cycle is defined by a pulse starting at SM, going through BS twice, and returning to SM. Because the optical field passes through the BS twice during each interaction with the atom, we adjust the parameter of BS to $\theta = \pi/2M$. In addition, SSC$_0$ is an empty single-side cavity. Except for the absence of atom, everything else is the same as SSC$_1$. C stands for optical circulator. PS stands for phase shifter. Unlike other components, the use of PS is only for the convenience of calculation and discussion. Its removal does not have a substantial impact on our method.

We assume that PS adds a π phase shift to the light field only as it propagates from BS to SSC. Its function can be described as $a_z^\dagger \rightarrow -a_z^\dagger$, where we still set $a_z^\dagger$ ($z = 0, 1$) as the creation operator of the light field in Zone z.

Initially, the light source emits a coherent pulse into the interferometer, while the light field in Zone 1 is in a vacuum state. As for the atom, it is prepared in a superposition state. Accordingly, the initial state of the entire system is $|\alpha, 0\rangle(|\uparrow\rangle + |\downarrow\rangle)/\sqrt{2}$. After m number of cycles, the wave-function of the whole system becomes (See the "System wave-function calculation" subsection in the Methods)

$$|\psi^{(2m)}\rangle = \frac{1}{\sqrt{2}}\left(|\alpha, 0\rangle|\uparrow\rangle + |\alpha\cos 2m\theta_M, \alpha\sin 2m\theta_M\rangle|\downarrow\rangle\right) \quad (1)$$

The dynamic evolution process of the system can be briefly described as follows. Due to the presence of the empty cavity SSC$_0$, when the atom is in $|\downarrow\rangle$, light field has no phase difference in Zones 0 and 1. Interference continues to occur, thereby generating $|-\alpha\rangle$. On the contrary, when the atom is in $|\uparrow\rangle$, the light field is frozen in $|\alpha\rangle$ due to the phase difference between the two Zones. Consequently, after M cycles, we have the light-atom entangled state $(|\alpha, 0\rangle|\uparrow\rangle + |-\alpha, 0\rangle|\downarrow\rangle)/\sqrt{2}$. We note that the light field is output from the SM$_0$ end and no photons appear at SM$_1$ side. After measuring the atom, the optical CS is deterministically prepared.

So far, we have only focused on the ideal case. In the following, we analyze the performance of our multiple reflection scheme for non-ideal situation. We show that our scheme is highly durable when it comes to parameters such as atomic spontaneous emission decay and atom-cavity detuning. The reason for this is the quantum Zeno effect caused by light absorption.

Experimental parameter analysis of multiple reflection scheme based on single-side cavity-atom coupling system

In the upcoming discussion, we utilize numerical simulations to analyze the impact of various practical parameters, including atomic, cavity parameters, the number of cycles, and the light loss rates of classical optical devices. We employ fidelity and cattiness[69–71] as metrics to assess the quality of the CS generated by our method. Additionally, recognizing the critical role of light loss in CS preparation[71], the two types of optical losses categorized in the introduction are the focus of our discussion. The first type is caused by the quantum system, specifically the atom-cavity interaction, while the second type solely originates from classical optical devices.

To begin with, we briefly outline the definitions of each parameter. Regarding the practical atom-cavity system (SSC$_1$), the incident light field is not only reflected, but also transmitted and scattered. To evaluate these effects, we set that 2γ and ω_a as the spontaneous emission decay rate and transition frequency of the atomic transition between $|e\rangle$ and $|\uparrow\rangle$, respectively. The coupling constant between the cavity mode of frequency ω_c and the atomic transition is g. The atom-cavity detuning is $\Delta = \omega_a - \omega_c$. Moreover, we set $\kappa_{R(T)}$ as the cavity field decay rate into the external light field on the CM$_{R(T)}$ side. Given that the atom is hardly excited in our scheme, as long as the condition of slowly varying light intensities is satisfied[37,45,72], SSC$_1$ can be well described by the input-output theory[73,74]. Suppose that $|\alpha_{i,1\uparrow}\rangle$ is the incident coherent light field from CM$_{R1}$ side when the atom is in $|\uparrow\rangle$. The cavity reflection $|\alpha_{R,1\uparrow}\rangle$ satisfies (See the "Input-output theory for the atom-cavity coupling system" subsection in the Methods)

$$\alpha_{R,1\uparrow} = \left[1 - \frac{2\kappa_R(i\Delta + \gamma)}{\kappa(i\Delta + \gamma) + g^2}\right]\alpha_{i,1\uparrow} = |\eta_{R,1\uparrow}|e^{i\beta_{R,1\uparrow}}\alpha_{i,1\uparrow} \quad (2)$$

where $\kappa = \kappa_R + \kappa_T$, $|\eta_{R,1\uparrow}|^2$ is the reflectivity and $\beta_{R,1\uparrow}$ describes the phase of the reflection. Similarly, for the transmission of the cavity $|\alpha_{T,1\uparrow}\rangle$, we have

$$\alpha_{T,1\uparrow} = -\frac{2(i\Delta + \gamma)\sqrt{\kappa_T\kappa_R}}{\kappa(i\Delta + \gamma) + g^2}\alpha_{i,1\uparrow} \quad (3)$$

Regarding the scattering field $|\alpha_{S,1\uparrow}\rangle$ due to the atomic spontaneous emission, we have

$$\alpha_{S,1\uparrow} = \frac{2g\sqrt{\kappa_R \gamma}}{\kappa(i\Delta + \gamma) + g^2}\alpha_{i,1\uparrow} \quad (4)$$

As for the situation that the atom is in $|\downarrow\rangle$, we still assume that the atom is completely unaffected by the cavity mode due to the large detuning. Therefore, SSC_1 in such case can be treated the same as the empty cavity SSC_0. By setting $g = 0$ in Eqs. (2)–(4), we can immediately obtain the corresponding reflection and transmission. As for the scattering light field, it is 0.

Before we continue our parameter analysis, let us make some necessary discussions about Eqs. (2)–(4). They constitute the mathematical foundation of the single reflection model, and seem unrelated to the intensity of the input light $|\alpha|^2$. It is true that the single reflection model allows for a certain degree of flexibility in $|\alpha|^2$. However, to derive Eqs. (2)–(4), the weak excitation approximation is required (see Eq. (15) in Methods), meaning that the light field inside the cavity cannot be too strong. This leads to the requirement that the cavity parameter κ_R not be too large, and similarly, the intensity of the incident field or the peak value of the incident pulse must also be constrained. In fact, when parameters such as κ_R, κ_T, γ, Δ, g and pulse length are fixed, increasing the intensity of the incident light always invalidates Eqs. (2)–(4). Consequently, to guarantee the single reflection model functions properly, further improvement of the system parameters is necessary. Overcoming these limitations is one of the objectives of our work. Our scheme ensures that the single-side cavity-atom coupling system can always work under the appropriate external field intensity. This effectively leads to avoid the difficulties brought about by improvement of the quantum system. From this perspective, our method is not a negation of the single reflection method. The core principle of our approach is to enhance and broaden the operational range of the atom-cavity coupling system. The two methods are complementing each other.

Based on Eqs. (2)–(4), we can numerically simulate the dynamic evolution of the input coherent pulse, and the fidelity of the output in the multiple reflection scheme. We suppose that the target state is $|\psi_T\rangle = (|\alpha\rangle|\uparrow\rangle + |-\alpha\rangle|\downarrow\rangle)/\sqrt{2}$, and the final state of the whole system after M cycles is $|\psi_f\rangle = (|C_{0\uparrow}\rangle|\text{loss}_\uparrow\rangle|\uparrow\rangle + |C_{0\downarrow}\rangle|\text{loss}_\downarrow\rangle|\downarrow\rangle)/\sqrt{2}$ with $|\text{loss}_{\uparrow(\downarrow)}\rangle = |C_{1\uparrow(\downarrow)}\rangle \otimes \prod_{m=1}^{M}|\alpha_{T,0\uparrow(\downarrow)}^{(m)}\rangle|\alpha_{S,0\uparrow(\downarrow)}^{(m)}\rangle|\alpha_{T,1\uparrow(\downarrow)}^{(m)}\rangle|\alpha_{S,1\uparrow(\downarrow)}^{(m)}\rangle$. Here state $|C_{z\uparrow(\downarrow)}\rangle$ ($z = 0, 1$) denotes the outputs appearing at SM_z side when the atom is in state $|\uparrow(\downarrow)\rangle$. $|\alpha_{T,z\uparrow(\downarrow)}^{(m)}\rangle$ denotes the transmission field generated by SSC_z in the m-th cycle, while $|\alpha_{S,z\uparrow(\downarrow)}^{(m)}\rangle$ denotes the scattering field. Given that $|\text{loss}_{\uparrow(\downarrow)}\rangle$ includes all optical losses caused by the atom-cavity coupling system, the fidelity is calculated by taking the trace of $|\text{loss}_{\uparrow(\downarrow)}\rangle$, i.e., $F = Tr_{\text{loss}}\{\langle\psi_T|\psi_f\rangle\langle\psi_f|\psi_T\rangle\} = \{|\langle\alpha|C_{0\uparrow}\rangle|^2 + |\langle-\alpha|C_{0\downarrow}\rangle|^2 + 2\text{Re}[\langle\alpha|C_{0\uparrow}\rangle\langle C_{0\downarrow}|-\alpha\rangle\langle\text{loss}_\downarrow|\text{loss}_\uparrow\rangle]\}/4$. In addition to fidelity F, we also investigate cattiness[69-71], $C_a = (|\langle\text{loss}_\uparrow|\text{loss}_\downarrow\rangle|^2 - |\langle C_{0\uparrow}|C_{0\downarrow}\rangle|^2)|C_{0\uparrow} - C_{0\downarrow}|^2/4$. Detailed calculations can be found in the "Cattiness calculation" subsection in the Methods. This physical quantity characterizes the purity of the prepared CS. Its maximum value is equal to $|\alpha|^2$. Apparently, C_a is more sensitive to light loss compared to F, since its value is related to $|\langle\text{loss}_\downarrow|\text{loss}_\uparrow\rangle|^2$, while F is solely related to $|\langle\text{loss}_\downarrow|\text{loss}_\uparrow\rangle|$.

As a comparison, we simulate the single reflection model[37] as well. More specifically, the input $|\alpha\rangle$ is directly reflected by SSC_1, and the corresponding output state is $(|\alpha_{R,1\uparrow}\rangle|\text{loss}_\uparrow\rangle|\uparrow\rangle + |\alpha_{R,1\downarrow}\rangle|\text{loss}_\downarrow\rangle|\downarrow\rangle)/\sqrt{2}$ with $|\text{loss}_{\uparrow(\downarrow)}\rangle = |\alpha_{T,1\uparrow(\downarrow)}\rangle|\alpha_{S,1\uparrow(\downarrow)}\rangle$. In this model, the constraints on the atomic parameters γ and Δ can be directly obtained from Eq. (2). For the empty cavity case (atom in $|\downarrow\rangle$), as long as $\kappa_T = 0$, the ideal reflection $\alpha_R = -\alpha_i$ can be obtained. As for the case where the atom is in $|\uparrow\rangle$, the condition for ideal reflection $\alpha_R = \alpha_i$ is $\Delta = \gamma = \kappa_T = 0$. If only γ is non-zero, we can see that the ideal reflection can be approximately achieved only when $\gamma \ll g^2/\kappa_R$. As γ increases, the cavity reflectivity $|\eta_{R,1\uparrow}|^2$ decreases monotonically until it drops to 0 when $\gamma = g^2/\kappa_R$. In other words, γ causes of the first type of light loss. If we focus on Δ, however, it only affects $\beta_{R,1\uparrow}$ when $\gamma = \kappa_T = 0$, since $|\eta_{R,1\uparrow}|^2 = 1$. As Δ varies from $-\infty$ to ∞, $\beta_{R,1\uparrow}$ decreases monotonically from π to $-\pi$. In order to ensure that $\beta_{R,1\uparrow}$ is close to 0, the constraint $\Delta \ll g^2/\kappa_R$ is required. Our subsequent numerical simulations will demonstrate that satisfying the constraints $\gamma \ll g^2/\kappa_R$ and $\Delta \ll g^2/\kappa_R$ is necessary for the single reflection model to function properly. In our multiple reflection scheme, however, the above constraints are relaxed.

Effect of atomic spontaneous emission decay rate γ. The atomic parameter γ is the primary source of the first type of light loss. To analyze its effect, we plot the fidelity F and cattiness C_a against $\tilde{\gamma} = \kappa_R\gamma/g^2$ with $g = 2\pi \times 7.8$ MHz, $\kappa_R = \kappa = 2\pi \times 2.3$ MHz and $\Delta = 0$ in Fig. 2, where $1/\tilde{\gamma}$ is the cooperativity. In this simulation, we assume that all classical optical devices such as SM are ideal. The yellow dotted-dashed curve is plotted for the single reflection model with $|\alpha|^2 = 4$, which has almost reached the upper limit of such model[37]. The remaining curves illustrate the multiple reflection model. Red curves correspond to $|\alpha|^2 = 4$, black to $|\alpha|^2 = 10$, and blue to $|\alpha|^2 = 16$. Dotted curves are used for $M = 5$, dashed curves for $M = 20$, solid curves for $M = 100$, and double-dotted-dashed curves for $M = 1000$. In addition, $\nu_{\max}$ is plotted in Fig. 2c for $M = 20$, where $\nu_{\max} = \max\{|\alpha_{i,1\uparrow}^{(1)}|^2, |\alpha_{i,1\uparrow}^{(2)}|^2, \ldots, |\alpha_{i,1\uparrow}^{(m)}|^2 \ldots\}$ is the maximum value of the average photon number reaching SSC_1 in each single cycle across all cycles when the atom is in $|\uparrow\rangle$. As shown in the figure, $\nu_{\max}$ is always less than 1 (For other M, the situation is similar), which validates the low atomic excitation probability condition, hence Eqs. (2)–(4) are valid for simulations.

By comparison, we can see that the multiple reflection scheme outperforms the single reflection scheme. In our scheme, it is evident that fidelity increases as M increases. Whereas for larger $|\alpha|^2$, larger M is required to achieve the same fidelity. More importantly, for γ much larger than $2\pi \times 3.0$ MHz (This value is taken from the experiment[37]. It corresponds to $\tilde{\gamma} \approx 0.11$ and has been marked in the figure), our scheme can still provide large F. To better explain the result, we consider the extreme case when $\tilde{\gamma} = 1$, which means all photons reaching SSC_1 in a single cycle are lost when the atom is in $|\uparrow\rangle$. Under such conditions, the interference between Zone 0 and Zone 1 is continuously interrupted, resulting in the output light field state in Zone 0 becomes $|\alpha\cos^2(\pi/2M)\cos^{M-1}2(\pi/2M)\rangle \approx |\alpha(1-\pi^2/2M)\rangle$[48,49], where the approximation is valid when M is sufficiently large. It is evident that when $M \gg |\alpha|$, the output photon state approaches $|\alpha\rangle$, signifying that the total light loss induced by the atom-cavity coupling system over the entire preparation process (M cycles) is actually significantly suppressed. This phenomenon is a manifestation of the quantum Zeno effect, which is caused by photon loss in the individual atom-cavity coupling system. We note that the cumulative loss is directly proportional to $|\alpha|^2$ and inversely proportional to M, which explains why in Fig. 2a, the larger M and the smaller $|\alpha|^2$, the better the fidelity. So far, our discussion is about $\tilde{\gamma} = 1$. As for the case of $0 < \tilde{\gamma} < 1$, the situation is similar. There is a mixture of two physical mechanisms. The first is to maintain the initial state by phase modulation, which does not cause any photon loss. The second is the quantum Zeno effect, which brings photon loss to the entire system. As $\tilde{\gamma}$ increases, the role of the second mechanism becomes increasingly important. Fortunately, by increasing M, the total loss can be greatly suppressed, which indicates that the quantum Zeno effect determines the lower bound of fidelity of our scheme. Together, the above two mechanisms ensure that our scheme has higher fidelity and higher tolerance to γ than the single reflection scheme as M increases. In addition, since the condition $\gamma \ll g^2/\kappa_R$ is relaxed, it implies that our scheme does not require strong coupling between atom and cavity when the value of γ is fixed.

Regarding cattiness, due to its greater sensitivity to light loss, achieving high cattiness requires much smaller light loss than the fidelity case. This necessitates a larger value of M. Consequently, we have plotted the blue double-dotted dashed curve for $|\alpha|^2 = 16$, $M = 1000$ in Fig. 2b. It is evident that

Fig. 2 | Influence of atomic spontaneous emission decay. a Fidelity F and (**b**) cattiness C_a versus dimensionless $\widetilde{\gamma} = \kappa_R \gamma / g^2$ with $g = 2\pi \times 7.8$ MHz, $\kappa_R = \kappa = 2\pi \times 2.3$ MHz and $\Delta = 0$. The yellow dotted-dashed curve represents the single reflection case. Other curves represent the multiple reflection case with different colors indicating different $|\alpha|^2$ and different styles indicating different M. **c** We plot ν_{max} versus $\widetilde{\gamma}$ when $M = 20$, where ν_{max} is the maximum value of the average photon number reaching SSC_1 in each single cycle across all cycles when the atom is in $|\uparrow\rangle$.
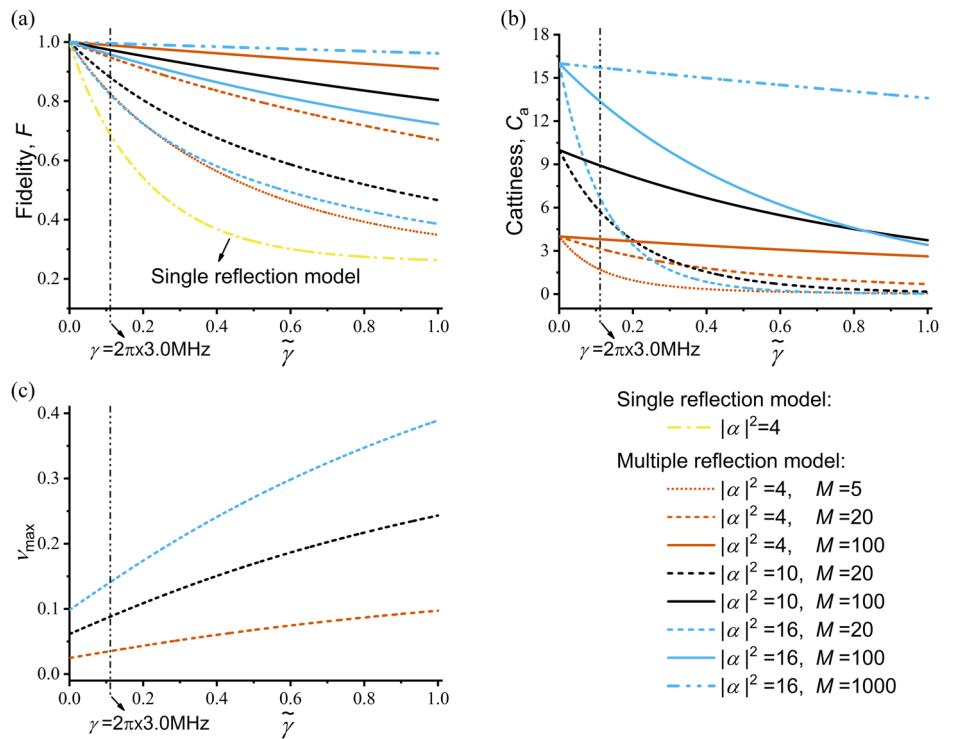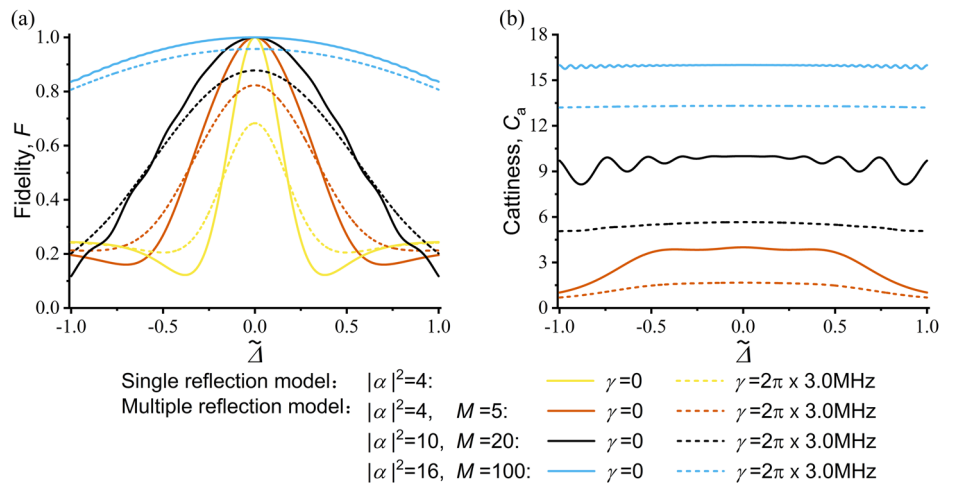

Fig. 3 | Influence of atom-cavity detuning. a Fidelity F and (**b**) cattiness C_a versus dimensionless $\widetilde{\Delta} = \kappa_R \Delta / g^2$ with $g = 2\pi \times 7.8$ MHz and $\kappa_R = \kappa = 2\pi \times 2.3$ MHz. The solid curves are plotted for $\gamma = 0$, and dashed curves are for $\gamma = 2\pi \times 3.0$ MHz. The yellow curves represent the single reflection model with $|\alpha|^2 = 4$, while other curves are for the multiple reflection scheme.


that even when the light loss in an individual atom-cavity coupling system is 100%, the cattiness can still exceed 10. In conjunction with our discussion on fidelity, even for significantly large values of $|\alpha|^2$, our scheme can ensure high fidelity and cattiness, provided the condition $M \gg |\alpha|$ is satisfied. This means that Type I loss does not limit the size of CS that our scheme can produce.

Effect of atom-cavity detuning Δ. Following the analysis of γ, we discuss the impact of Δ. We have shown that by interrupting the interference, the transmission of the light field from Zone 0 to Zone 1 can be suppressed. Note that the phase mismatch between the two Zones also interrupts the interference, we expect that our scheme can have high tolerance of Δ as well. In Fig. 3, we plot fidelity F and cattiness C_a against $\widetilde{\Delta} = \kappa_R \Delta / g^2$. Solid curves are plotted for $\gamma = 0$. Dashed curves are for $\gamma = 2\pi \times 3.0$ MHz. The values of g, κ_R and κ_T are the same as in Fig. 2. In addition, the yellow curves are plotted for the single reflection model with $|\alpha|^2 = 4$. As for the multiple reflection model, the red curves are for

$|\alpha|^2 = 4$, $M = 5$, the black curves are for $|\alpha|^2 = 10$, $M = 20$ and the blue curves are for $|\alpha|^2 = 16$, $M = 100$, respectively. As shown in Fig. 3, even for large $|\alpha|$, as long as M is large, our scheme can be less sensitive to Δ. Moreover, since Δ does not induce optical losses, the responses of F and C_a to different M are consistent.

Effect of the atomic decoherence. Besides the atomic parameters γ and Δ, next we provide a discussion about the influence of the decoherence between the atomic states $|\downarrow\rangle$ and $|\uparrow\rangle$. Obviously, our scheme requires the atom to remain in superposition at least until the end of M cycles. Nevertheless, we need to mention that the multiple reflection processes hardly affect the atomic decoherence. In our scheme, when the atom is in $|\uparrow\rangle$, the low atomic excitation probability can be satisfied. As for the atom in $|\downarrow\rangle$, it is not coupled to the light field. We note that the atomic superposition state has been reported to last about 400 μs[75,76], whereas the full-width at half-maximum of the light pulse that is employed in the

Fig. 4 | Influence of light loss caused by classical optical devices. a Effective fidelity F_{ef}, (**b**) cattiness C_a, and (**c**) the output intensity $|\alpha_{ef}|^2$ versus ε with $g = 2\pi \times 7.8$ MHz, $\gamma = 2\pi \times 3.0$ MHz, $\kappa_R = \kappa = 2\pi \times 2.3$ MHz, and $\Delta = 0$. The yellow dotted-dashed curves represent the single reflection model with $|\alpha|^2 = 4$, and other curves represent the multiple reflection scheme with different $|\alpha|^2$ and M. The target state is $(|\alpha_{ef}\rangle|\uparrow\rangle + |-\alpha_{ef}\rangle|\downarrow\rangle)/\sqrt{2}$.
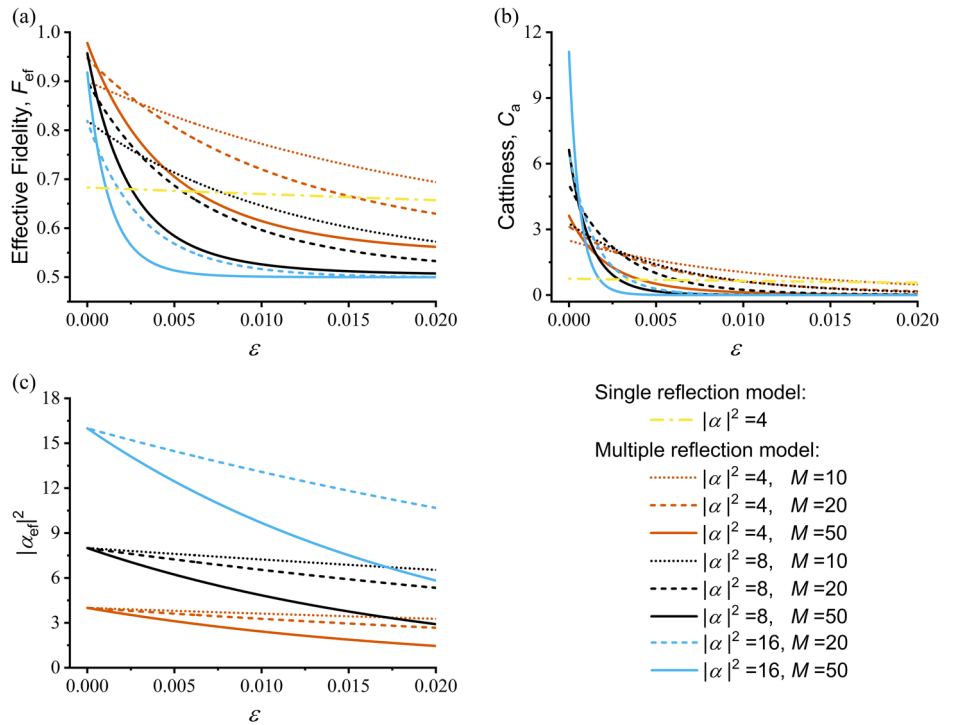
experiment of single reflection model is 2.3 μs[37]. Therefore, it is possible for our scheme to be completed before the decoherence.

Effect of light loss caused by classical optical devices ε. So far, we have primarily discussed atomic parameters and optical losses due to atom (Type I loss). Next, we explore the impact of Type II loss, caused by classical optical devices, while keeping Type I light loss constant. We postulate that the loss rate per cycle outside the cavity is denoted by ε. Accordingly, the cumulative loss rate over the entire preparation process can be approximated as $M\varepsilon$, given that $(1 - \varepsilon)^M \approx 1 - M\varepsilon$ under the assumption of a small ε. Furthermore, considering the symmetrical of the optical devices on both arms of the interferometer, it is reasonable to assume that Type II loss is identical for each arm. Consequently, ε can be expressed as the sum of the light losses from each optical device located on a single arm of the interferometer. To facilitate our discussion, we assume that all optical devices are ideal, except for the switchable mirror SM (We also assume that irrespective of whether SM is turned on or off, its light loss rate remains constant). When coherent light $|\beta_z\rangle$ incident upon SM_z ($z = 0,1$), the reflected field is denoted as $|\sqrt{1 - \varepsilon}\beta_z\rangle$, and the lost light field can be represented as $|\sqrt{\varepsilon}\beta_z\rangle$. In our simulation, the effect of these loss terms $|\sqrt{\varepsilon}\beta_z\rangle$ from different cycles is accounted for by taking the trace, similar to our treatment of the cavity mentioned earlier.

In Fig. 4, we plot ε against effective fidelity $F_{ef} = Tr_{loss}\{\langle\psi_{ef}|\psi_f\rangle\}$, cattiness C_a, and output intensity $|\alpha_{ef}|^2$ for different $|\alpha|^2$ and M. Here, F_{ef} differs from F in that the target state is set as $|\psi_{ef}\rangle = (|\alpha_{ef}\rangle|\uparrow\rangle + |-\alpha_{ef}\rangle|\downarrow\rangle)/\sqrt{2}$ with $\alpha_{ef} = -C_{0\downarrow} = \alpha[(\kappa_R - \kappa_T)/(\kappa_T + \kappa_R)]^M$. Note that $|C_{0\downarrow}\rangle$ is the output when the atom is in $|\downarrow\rangle$, where interference occurs between the two empty cavities. If the optical parameters of these two cavities are the same, only intensity of the output is affected and reduced from $|\alpha|^2$ to $|\alpha_{ef}|^2$. For the cavity-atom system, the parameters are set as $g = 2\pi \times 7.8$ MHz, $\kappa_R = 2\pi \times 2.3$ MHz, and $\gamma = 2\pi \times 3.0$ MHz, aligning with actual cavity characteristics. However, for κ_T, we set it to zero. Based on the above parameters, the corresponding Type I loss is about 36.6%. Before we begin analyzing the impact of Type II light loss, it is important to note that the role of κ_T can be simulated with ε, since the main impact of κ_T is on the empty cavity light loss. This loss can be added to other Type II losses. Therefore,

here we simply treat it as 0. Detailed explanations regarding κ_T are provided later.

For comparison, we have also plotted the curves corresponding to the single reflection model with $|\alpha|^2 = 4$ (the yellow dotted-dashed curves). In this scenario, both F_{ef} and C_a demonstrate minimal impact from ε, indicating that the key factor affecting the single reflection model here primarily stems from the optical losses in the individual atom-cavity system (Type I light loss). In this context, we utilize the yellow curve as a baseline to assess the quality of CS preparation in the multiple reflection model. From Fig. 4a, b, it can be observed that when ε is large, the multiple reflection model suffers from Type II light loss, with both F_{ef} and C_a falling below that of the single reflection model. As M increases, the situation deteriorates further. However, as ε decreases, a dramatic shift occurs. Both F_{ef} and C_a begin to outperform the single reflection case and rapidly increase. Smaller values of $|\alpha|^2$ and M exhibit a higher tolerance to Type II light loss, but larger M values can achieve greater maximal values of F_{ef} and C_a (at $\varepsilon = 0$). As a result, there are observable intersections of curves for different M values for a given $|\alpha|^2$, which implies that it's possible to obtain better fidelity using higher M. For larger values of $|\alpha|^2$, such improvements due to M are only noticeable when ε is closer to zero. All these observed effects are because that the impact of Type I losses gradually becomes dominant as ε approaches zero, and our method effectively suppresses the influence of Type I light loss. It's important to recognize that in the single reflection model, Type I light losses can only be reduced through improvements in the atom-cavity system. In contrast, our multiple reflection approach, while not immune to light losses from classical optical devices, offers a method to reduce the stringent requirements on quantum microscopic system. This is the central and distinctive feature of our work.

To pave the way for the initiation of proof-of-concept experiments, we also provide two tables specifying the loss tolerances for classical optical devices in a single cycle. These loss tolerances are required to achieve certain levels of effective fidelity and cattiness under varying conditions of $|\alpha|^2$ and M. The tables reveal that, to achieve over 70% effective fidelity in conditions with $|\alpha|^2 \leq 4$ and $M \leq 10$, our scheme's tolerance for Type II loss can be close to or even exceed 2%. For larger $|\alpha|^2$, however, our scheme requires much smaller ε. Hence, for our scheme, the constraint on preparing large-sized CS is tied to the quality of classical optical devices.

Fig. 5 | Influence of cavity parameters. a, b Effective fidelity F_{ef}, (**c, d**) cattiness C_a, and the output intensity $|\alpha_{ef}|^2$ versus κ_R with varying g, M, and κ_T in the multiple reflection model, where other parameters are set as $|\alpha|^2 = 8$, $\gamma = 2\pi \times 3.0$ MHz, and $\Delta = 0$. The target state is $(|\alpha_{ef}\rangle|\uparrow\rangle + |-\alpha_{ef}\rangle|\downarrow\rangle)/\sqrt{2}$. Solid curves represent $\kappa_T = 2\pi \times 0.02$ MHz, and dashed curves represent $\kappa_T = 2\pi \times 0.002$ MHz. The green curves are plotted for $|\alpha_{ef}|^2$ only, while curves in other colors represent F_{ef} and C_a. Black corresponds to $g = 2\pi \times 7.8$ MHz, red to $g = 2\pi \times 15$ MHz, and blue to $g = 2\pi \times 30$ MHz.
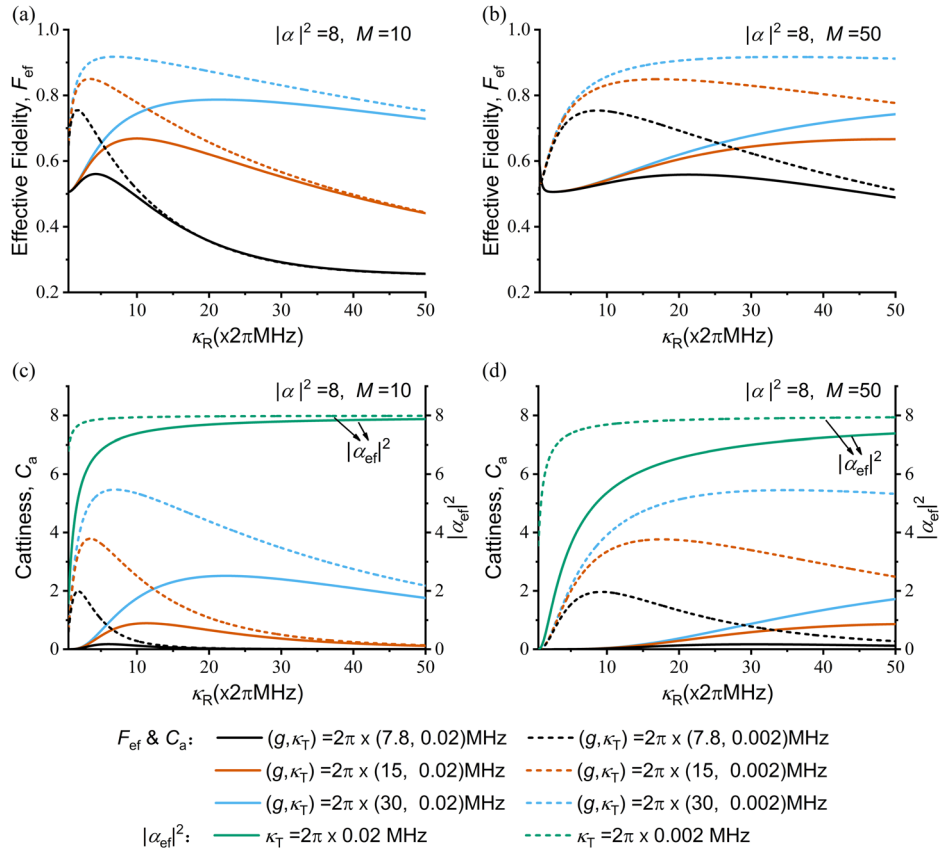
Discussion on the cavity parameter κ_T and potential approaches to reduce light loss in empty cavity. Next, we provide additional explanation and clarification on the role of κ_T. We note that κ_T causes light loss when the atom is in either $|\uparrow\rangle$ or $|\downarrow\rangle$, thus affecting both the first and second types of light loss. However, when the atom is in $|\uparrow\rangle$, according to Eqs. (3)–(4), and the fact that $g > \gamma \gg \kappa_T$[37], the loss caused by light field passing through the atom-cavity coupling system (Eq. (3)) is much smaller than the light loss caused by atomic scattering (Eq. (4)). As for Eq. (4), since $\kappa_T \ll \kappa_R$, the influence of κ_T can be neglected. Hence, the Type I light loss due to κ_T is not our primary concern. In the scenario where the atom is in $|\downarrow\rangle$ and does not participate in the interaction, the light transmission through the empty cavity falls under Type II light loss. In other words, the effect of κ_T can be accounted for in ε. According to Eq. (2), the light loss rate of the empty cavity after a single reflection is $1 - |(\kappa_T - \kappa_R)/(\kappa_T + \kappa_R)|^2$. In the experiment[37], the cavity parameters are $\kappa_T = 2\pi \times 0.2$ MHz and $\kappa_R = 2\pi \times 2.3$ MHz, which results in $\varepsilon \approx 29\%$ even if other optical devices are ideal, while after a few reflections, almost all photons are lost. Therefore, this cavity is unfortunately not suitable for our scheme. To reduce the optical losses, one needs either decrease κ_T or increase κ_R. The latter is simpler in practice. However, although increasing κ_R can reduce photon loss during the interference of two empty cavities (The atom is in state $|\downarrow\rangle$), it also increases photon loss in the presence of atom-cavity coupling (The atom is in state $|\uparrow\rangle$). To verify this, we plot Fig. 5 with $|\alpha|^2 = 8$, $\gamma = 2\pi \times 3.0$ MHz, and $\Delta = 0$. In Fig. 5a (for $M = 10$) and 5b (for $M = 50$), we plot the effective fidelity F_{ef} against κ_R. Solid curves represent $\kappa_T = 2\pi \times 0.02$ MHz, while dashed curves represent $\kappa_T = 2\pi \times 0.002$ MHz. The corresponding light loss rate of the empty cavity is approximately 3.4% for $\kappa_T = 2\pi \times 0.02$ MHz and 0.35% for $\kappa_T = 2\pi \times 0.002$ MHz when $\kappa_R = 2\pi \times 2.3$ MHz. Black curves are for $g = 2\pi \times 7.8$ MHz, red for $g = 2\pi \times 15$ MHz, and blue for $g = 2\pi \times 30$ MHz. As for Fig. 5c, d, the green curves are plotted for $|\alpha_{ef}|^2$, while curves of other colors represent C_a. It is observed that F_{ef} can be significantly improved as κ_T decreases. Regarding κ_R, as it initially increases, $|\alpha_{ef}|^2$

rapidly rises to its maximum value 8, which causes F_{ef} to increase. Subsequently, photon loss due to atom-cavity coupling plays a major role, resulting in the decrease of F_{ef}. Particularly, it's noteworthy that for the black solid curve, when F_{ef} starts to decrease, its corresponding $|\alpha_{ef}|^2$ is not close to 8. The reason is that κ_R is approaching the limit g^2/γ. Under such limit, the photon loss of a single reflection on SSC$_1$ when the atom is in $|\uparrow\rangle$ is almost 100%. Therefore, we choose larger values of g to raise the limit so that the corresponding $|\alpha_{ef}|^2$ of maximum F_{ef} can get closer to the maximum value 8, thereby increasing F_{ef}. This phenomenon is verified in Fig. 5. Moreover, in the blue curves, κ_R maintains a wide range of high fidelity. This is due to relaxed constraint of $g^2 \gg \kappa_R\gamma$ in our scheme. However, we must emphasize that achieving high fidelity does not necessarily require increasing g. By decreasing κ_T, we can achieve the same purpose. In fact, the motivation of this work is to reduce the influence of the atom, and to show that the performance of our protocol can be improved by just upgrading the classical optical system, such as the parameters κ_T and ε.

Regarding the impact of M, we provide a brief explanation here. When κ_R is small, significant Type II light loss leads to a decrease in our scheme's performance with larger M values, as depicted in Fig. 5. However, as κ_R increases, leading to a decrease in Type II light loss, larger M values can ultimately offer improved F_{ef} and C_a.

Discussion on pulse length and interferometer size. Based on the above analysis of various experimental parameters, we now discuss the requirements of our scheme for the duration of the incident pulse. It is noteworthy that the influence of the atom-cavity coupling system on the wave packet waveshape during a single reflection process has been discussed[42]. The results indicate that to shorten the pulse length by half, while maintaining the reflected waveshape unchanged is necessary to double κ_R. For the single reflection model, an increase in κ_R amplifies Type I losses, resulting in reduced fidelity, hence is not a favorable option. In our scheme, however, since Type I losses can be mitigated, increasing

κ_R is feasible. For example, in the experiment[37], the pulse duration is $T_P = 2.3$ μs, and the cavity parameter κ_R is $2\pi \times 2.3$ MHz. According to our simulations in Fig. 5, when $|\alpha|^2 = 8$, $M = 50$, $\kappa_T = 2\pi \times 0.002$ MHz, and $\kappa_R = 2\pi \times 10$ MHz, the effective fidelity of the output CS in our scheme is about 0.75. With κ_R increased by approximately 5 times, the pulse length used in our scheme can be shortened 5 times under the condition of keeping waveshape unchanged, i.e., to $T_P \approx 0.5$ μs.

We, so far, stipulated that the waveshape of the reflected pulse remains unchanged. This is a requirement from the single reflection model, but not a necessity in our scheme. This is due to the fact that when the atom is in $|\downarrow\rangle$, interference occurs between the two empty cavities, and even if the reflected waveshape distorts, it does not affect the interference process. Conversely, when the atom is in $|\uparrow\rangle$, the role of the atom is merely to disrupt the interference. In this case, the light field is primarily concentrated on the empty cavity side, and the waveshape of the reflected pulse is still determined by the empty cavity reflection. Consequently, variations in the waveshape of the output pulse do not affect the generation of CS. This facilitates further compression of the pulse length in our scheme.

Next, we briefly discuss the size of the interferometer. If we define the size of the interferometer by the distance L between SM_0 and SSC_0, to ensure that the light-matter interaction in two cycles does not interfere with each other, it implies that L needs to be greater than the half pulse length, i.e., $L \geq (T_P c)/2$, where c is the speed of light. Hence, the total flight distance of the pulse in the entire CS preparation process is $MT_P c$. For a pulse duration $T_P = 2.3$ μs, L needs to be at least 350 m, and the total flight distance falls within the kilometer scale. Given such distances, employing optical fibers to construct the interferometer is a reasonable choice. Regarding the requirements for light loss from classical optical devices, one can refer to Tables 1 and 2 we provided. We note that the

parameter κ_R in these tables is specified as $2\pi \times 2.3$ MHz. Increasing it allows us to further compress the pulse duration. For instance, setting κ_R to $2\pi \times 10$ MHz results in a pulse duration T_P of 0.5 μs, with minimum L adjusted to 75 m. By fixing other parameters at $(g, \gamma) = 2\pi \times (7.8, 3.0)$ MHz and $\kappa_T = \Delta = 0$, along with using $M = 20$ and the best-reported optical fiber, which has an average attenuation of less than 0.157 dB km^{-1}[77] (the corresponding Type II loss is about 0.53%), the effective fidelity of the output CS is about 0.77 for an input light field of $|\alpha|^2 = 3$. In this estimate, we have not yet accounted for other classical optical losses, such as those from SM and fiber-cavity coupling. If we set these additional losses to 2%, the effective fidelity reduces to 0.63. While our scheme can shift the source of errors from the atomic system to classical optical systems, it also demands higher manufacturing technology standards for existing optical devices.

Lastly, we address the requirements for the SM. In addition to light loss restrictions, there are also requirements for its response time T_s. One promising candidate of SM is Pockels cell[65–68]. Applying high voltage, it can rotate the polarization of the light field by 90 degrees, facilitating the extraction of the light field from the interferometer. Its response time is in the nanosecond range. Hence, T_s can be significantly shorter than the duration of the pulse T_P. Strictly speaking, to ensure that the transmission of the pulse is uninterrupted, the length of L should be $(T_P + T_s)c/2$, which means there needs to be a sufficient time window allowed for the change of state in the Pockels Cell. However, since $T_s \ll T_P$, L is primarily determined by T_P.

Conclusions

We propose a method for generating macro-micro entanglement based on the interaction-free measurement and the quantum Zeno effect. Our

Table 1 | Impact of classical optical devices on fidelity

Effective fidelity		$F_{ef} \geq 70\%$	$F_{ef} \geq 80\%$	$F_{ef} \geq 90\%$	$F_{ef} \geq 95\%$
$|\alpha|^2$	M	ε	ε	ε	ε
3	6	$\leq 3.91 \times 10^{-2}$ ($|\alpha_{ef}|^2 = 2.36$)	$\leq 1.31 \times 10^{-2}$ ($|\alpha_{ef}|^2 = 2.77$)		
3	10	$\leq 2.95 \times 10^{-2}$ ($|\alpha_{ef}|^2 = 2.22$)	$\leq 1.21 \times 10^{-2}$ ($|\alpha_{ef}|^2 = 2.66$)	1.87×10^{-3} ($|\alpha_{ef}|^2 = 2.94$)	
4	8	$\leq 2.14 \times 10^{-2}$ ($|\alpha_{ef}|^2 = 3.36$)	$\leq 7.31 \times 10^{-3}$ ($|\alpha_{ef}|^2 = 3.77$)		
4	10	$\leq 1.91 \times 10^{-2}$ ($|\alpha_{ef}|^2 = 3.30$)	$\leq 7.36 \times 10^{-3}$ ($|\alpha_{ef}|^2 = 3.72$)	$\leq 2.38 \times 10^{-5}$ ($|\alpha_{ef}|^2 = 4.00$)	
4	50	$\leq 5.18 \times 10^{-3}$ ($|\alpha_{ef}|^2 = 3.08$)	$\leq 2.53 \times 10^{-3}$ ($|\alpha_{ef}|^2 = 3.52$)	$\leq 9.17 \times 10^{-4}$ ($|\alpha_{ef}|^2 = 3.82$)	$\leq 3.05 \times 10^{-4}$ ($|\alpha_{ef}|^2 = 3.94$)
8	20	$\leq 4.53 \times 10^{-3}$ ($|\alpha_{ef}|^2 = 7.31$)	$\leq 1.81 \times 10^{-3}$ ($|\alpha_{ef}|^2 = 7.71$)		
8	50	$\leq 2.22 \times 10^{-3}$ ($|\alpha_{ef}|^2 = 7.16$)	$\leq 1.09 \times 10^{-3}$ ($|\alpha_{ef}|^2 = 7.58$)	$\leq 3.36 \times 10^{-4}$ ($|\alpha_{ef}|^2 = 7.87$)	$\leq 3.96 \times 10^{-5}$ ($|\alpha_{ef}|^2 = 7.98$)
16	50	$\leq 9.47 \times 10^{-4}$ ($|\alpha_{ef}|^2 = 15.3$)	$\leq 4.18 \times 10^{-4}$ ($|\alpha_{ef}|^2 = 15.7$)	$\leq 5.50 \times 10^{-5}$ ($|\alpha_{ef}|^2 = 16.0$)	

We specify the tolerance to light loss (ε) required by classical optical devices in a single cycle to achieve a specific effective fidelity (F_{ef}) across various $|\alpha|^2$ and M values. The corresponding output light intensity $|\alpha_{ef}|^2$ is indicated in parentheses. The parameters are set as $(g, \gamma, \kappa_R) = 2\pi \times (7.8, 3.0, 2.3)$ MHz and $\kappa_T = \Delta = 0$.

Table 2 | Impact of classical optical devices on cattiness

Cattiness		$Ca \geq 50\%|\alpha|^2$	$Ca \geq 60\%|\alpha|^2$	$Ca \geq 70\%|\alpha|^2$	$Ca \geq 80\%|\alpha|^2$
$|\alpha|^2$	M	ε	ε	ε	ε
3	6	$\leq 2.48 \times 10^{-3}$ ($|\alpha_{ef}|^2 = 2.96$)			
3	10	$\leq 4.67 \times 10^{-3}$ ($|\alpha_{ef}|^2 = 2.86$)	$\leq 2.02 \times 10^{-3}$ ($|\alpha_{ef}|^2 = 2.94$)		
4	8	$\leq 1.53 \times 10^{-3}$ ($|\alpha_{ef}|^2 = 3.95$)			
4	10	$\leq 2.43 \times 10^{-3}$ ($|\alpha_{ef}|^2 = 3.90$)	$\leq 4.13 \times 10^{-4}$ ($|\alpha_{ef}|^2 = 3.98$)		
4	50	$\leq 1.37 \times 10^{-3}$ ($|\alpha_{ef}|^2 = 3.73$)	$\leq 9.37 \times 10^{-4}$ ($|\alpha_{ef}|^2 = 3.82$)	$\leq 5.79 \times 10^{-4}$ ($|\alpha_{ef}|^2 = 3.89$)	$\leq 2.76 \times 10^{-4}$ ($|\alpha_{ef}|^2 = 3.95$)
8	20	$\leq 6.81 \times 10^{-4}$ ($|\alpha_{ef}|^2 = 7.89$)	$\leq 1.45 \times 10^{-4}$ ($|\alpha_{ef}|^2 = 7.98$)		
8	50	$\leq 6.04 \times 10^{-4}$ ($|\alpha_{ef}|^2 = 7.76$)	$\leq 3.83 \times 10^{-4}$ ($|\alpha_{ef}|^2 = 7.85$)	$\leq 1.99 \times 10^{-4}$ ($|\alpha_{ef}|^2 = 7.92$)	$\leq 4.12 \times 10^{-5}$ ($|\alpha_{ef}|^2 = 7.98$)
16	50	$\leq 1.99 \times 10^{-4}$ ($|\alpha_{ef}|^2 = 15.8$)	$\leq 8.83 \times 10^{-5}$ ($|\alpha_{ef}|^2 = 15.9$)		

We specify the tolerance to light loss (ε) required by classical optical devices in a single cycle to achieve a specific cattiness (C_a) across various $|\alpha|^2$ and M values. The corresponding output light intensity $|\alpha_{ef}|^2$ is indicated in parentheses. The parameters are set as $(g, \gamma, \kappa_R) = 2\pi \times (7.8, 3.0, 2.3)$ MHz and $\kappa_T = \Delta = 0$.

method allows for the deterministic preparation of optical CS with arbitrarily large average photon numbers. Because only a small fraction of photons actually interacts with the quantum microsystem during multiple interactions, our method avoids directly exposing the quantum microsystem to a strong light field. This indirect control mechanism is a key feature of our work. Another significant feature of our work is the tolerance it shows for photon loss within the quantum microsystem. We show that the state $|-\alpha\rangle$ is generated through multiple optical interferences, independent of the quantum microsystem. Conversely, the state $|\alpha\rangle$ results from the disruption of the interference process, which remains feasible even if the quantum microsystem experiences substantial photon loss or other imperfections. This fact enables our scheme to improve the fidelity of the output CS through enhancements to the classical optical system.

Methods
System wave-function calculation
We have mentioned that a_0 and a_1 represent the annihilation operators of the light field in Zone 0 and Zone 1, respectively. Based on this, the function of BS can be described as $a_0^\dagger \to a_0^\dagger \cos\theta + a_1^\dagger \sin\theta$ and $a_1^\dagger \to a_1^\dagger \cos\theta - a_0^\dagger \sin\theta$ where $\theta = \pi/2M$. Now, we consider an arbitrary initial photon state

$$|\text{Initial}\rangle = |u, v\rangle = \exp\left(ua_0^\dagger - u^*a_0\right)\exp\left(va_1^\dagger - v^*a_1\right)|0, 0\rangle \quad (5)$$

which represents that a coherent state $|u\rangle$ is in Zone 0 and a coherent state $|v\rangle$ is in Zone 1. After passing through the BS, we have the final state

$$\begin{aligned}|\text{Final}\rangle &= \exp\left[u\left(a_0^\dagger\cos\theta + a_1^\dagger\sin\theta\right) - u^*\left(a_0\cos\theta + a_1\sin\theta\right)\right], \\ &\times \exp\left[v\left(a_1^\dagger\cos\theta - a_0^\dagger\sin\theta\right) - v^*\left(a_1\cos\theta - a_0\sin\theta\right)\right]|0, 0\rangle \\ &= |u\cos\theta - v\sin\theta, u\sin\theta + v\cos\theta\rangle\end{aligned} \quad (6)$$

Similarly, consider an arbitrary phase operation $a^\dagger \to e^{i\varphi}a^\dagger$. For the initial state $|\text{Initial}\rangle = |u\rangle$, after the operation, the final state is

$$\begin{aligned}|\text{Final}\rangle &= \exp\left(-\frac{1}{2}|u|^2\right)\sum_{n=0}^{\infty}\frac{u^n}{\sqrt{n!}}\frac{1}{\sqrt{n!}}\left(e^{i\varphi}a^\dagger\right)^n|0\rangle \\ &= \exp\left(-\frac{1}{2}|u|^2\right)\sum_{n=0}^{\infty}\frac{1}{\sqrt{n!}}\left(ue^{i\varphi}\right)^n|n\rangle = |ue^{i\varphi}\rangle\end{aligned} \quad (7)$$

Based on Eqs. (6) and (7), we provide the calculation of Eq. (1).

At the beginning of the preparation, the wave-function of the whole system is

$$|\psi^{(0)}\rangle = \frac{\sqrt{2}}{2}|\alpha, 0\rangle\left(|\uparrow\rangle + |\downarrow\rangle\right) \quad (8)$$

In the first cycle, after the photons pass through BS for the first time, the system state is

$$|\psi^{(1)}\rangle = \frac{\sqrt{2}}{2}|\alpha\cos\theta, \alpha\sin\theta\rangle\left(|\uparrow\rangle + |\downarrow\rangle\right) \quad (9)$$

Before the photons are reflected by SSC, the system state becomes $\frac{\sqrt{2}}{2}|-\alpha\cos\theta, -\alpha\sin\theta\rangle\left(|\uparrow\rangle + |\downarrow\rangle\right)$ due to PS. Regarding the reflection, we emphasize that only when the atom is in $|\uparrow\rangle$, SSC_1 does not change the phase of the reflected field. As a result, the wave function of

the whole system becomes $\frac{\sqrt{2}}{2}|\alpha\cos\theta, -\alpha\sin\theta\rangle|\uparrow\rangle + \frac{\sqrt{2}}{2}|\alpha\cos\theta, \alpha\sin\theta\rangle|\downarrow\rangle$. Subsequently, after the second time that the photons pass through BS, we have

$$|\psi^{(2)}\rangle = \frac{\sqrt{2}}{2}|\alpha, 0\rangle|\uparrow\rangle + \frac{\sqrt{2}}{2}|\alpha\cos 2\theta, \alpha\sin 2\theta\rangle|\downarrow\rangle \quad (10)$$

This state becomes the initial state of the second cycle, and the process is repeated. It is not difficult to obtain that after m cycles, the wave-function of the whole system is

$$|\psi^{(2m)}\rangle = \frac{\sqrt{2}}{2}|\alpha, 0\rangle|\uparrow\rangle + \frac{\sqrt{2}}{2}|\alpha\cos 2m\theta, \alpha\sin 2m\theta\rangle|\downarrow\rangle \quad (11)$$

Here the superscript of $|\psi^{(2m)}\rangle$ represents the photons pass through BS $2m$ times.

Input-output theory for the atom-cavity coupling system
The Hamiltonian of cavity-atom system (SSC_1) can be described as

$$\begin{aligned}H &= \hbar\omega_e\sigma_{ee} + \hbar\omega_\uparrow\sigma_{\uparrow\uparrow} + \hbar\omega_c a^\dagger a + \hbar\sum_{J=R,T,S}\int_{-\infty}^{\infty}\omega_J b_J^\dagger(\omega_J)b_J(\omega_J)d\omega_J \\ &+ \hbar g\left(\sigma_{\uparrow e}a^\dagger + \sigma_{e\uparrow}a\right) + \hbar\sqrt{\frac{\gamma}{\pi}}\int_{-\infty}^{\infty}\left[\sigma_{\uparrow e}b_S^\dagger(\omega_S) + \sigma_{e\uparrow}b_S(\omega_S)\right]d\omega_S \\ &+ i\hbar\sqrt{\frac{\kappa_R}{\pi}}\int_{-\infty}^{\infty}\left[ab_R^\dagger(\omega_R) - a^\dagger b_R(\omega_R)\right]d\omega_R \\ &+ i\hbar\sqrt{\frac{\kappa_T}{\pi}}\int_{-\infty}^{\infty}\left[ab_T^\dagger(\omega_T) - a^\dagger b_T(\omega_T)\right]d\omega_T\end{aligned} \quad (12)$$

where $\hbar\omega_e$ is the energy of excited atomic state $|e\rangle$, $\hbar\omega_\uparrow$ is the energy of the atomic state $|\uparrow\rangle$, ω_c is the frequency of the cavity mode described by annihilation operator a, ω_J is the frequency of external field described by annihilation operator $b(\omega_{J=R,T,S})$ with $\left[b_J(\omega_J), b_J^\dagger(\omega_J')\right] = \delta(\omega_J - \omega_J')$, and the subscript R represents the external multi-mode field on CM_R side, T represents the external field on CM_T side, S represents the scattering field due to the atomic spontaneous emission. In addition, g is coupling constant between the cavity and the atomic transition between $|e\rangle$ and $|\uparrow\rangle$, 2γ is the spontaneous atomic decay rate on the same transition, κ_R and κ_T are cavity field decay rates. We also set that $\sigma_{\uparrow e} = |\uparrow\rangle\langle e|$, $\sigma_{ee} = |e\rangle\langle e|$ and $\sigma_{\uparrow\uparrow} = |\uparrow\rangle\langle\uparrow|$.

Based on the above Hamiltonian, it is not difficult to obtain the following Heisenberg equations

$$\frac{da(t)}{dt} = -i\omega_c a(t) - ig\sigma_{\uparrow e}(t) - \sum_{J=R,T}\sqrt{\frac{\kappa_J}{\pi}}\int_{-\infty}^{\infty}b_J(\omega_J, t)d\omega_J \quad (13)$$

$$\begin{aligned}\frac{d}{dt}\sigma_{\uparrow e}(t) &= -i\left(\omega_e - \omega_\uparrow\right)\sigma_{\uparrow e}(t) + ig\left[\sigma_{ee} - \sigma_{\uparrow\uparrow}(t)\right]a(t) \\ &+ i\sqrt{\frac{\gamma}{\pi}}\int_{-\infty}^{\infty}\left[\sigma_{ee}(t) - \sigma_{\uparrow\uparrow}(t)\right]b_S(\omega_S, t)d\omega_S \\ &\approx -i\left(\omega_e - \omega_\uparrow\right)\sigma_{\uparrow e}(t) - iga(t) - i\sqrt{\frac{\gamma}{\pi}}\int_{-\infty}^{\infty}b_S(\omega_S, t)d\omega_S\end{aligned} \quad (14)$$

In the approximation, we have assumed that[37,45,72]

$$\left\langle\left(\sigma_{ee} - \sigma_{\uparrow\uparrow}\right)a\right\rangle = -\langle a\rangle \quad (15)$$

which indicates that the atom stays in the state $|\uparrow\rangle$ most of the time. This can be satisfied when the input is weak.

In addition, we can also obtain Heisenberg equations for $b(\omega)$. They are

$$\frac{db_J(\omega_J, t)}{dt} = -i\omega_J b_J(\omega_J, t) + \sqrt{\frac{\kappa_R}{\pi}} a(t), J = R, T \quad (16)$$

$$\frac{db_S(\omega_S, t)}{dt} = -i\omega_S b_S(\omega_S, t) - i\sqrt{\frac{\gamma}{\pi}} \sigma_{\uparrow e}(t) \quad (17)$$

Equations (16) and (17) can be rewritten in integral form. If we assume that the atom-light interaction begins at time $T_{in} < t$, we have

$$b_J(\omega_J, t) = b_J(\omega_J, T_{in}) e^{i\omega_J(T_{in}-t)} + \sqrt{\frac{\kappa_J}{\pi}} \int_{T_{in}}^t a(t') e^{i\omega_J(t'-t)} dt' \quad (18)$$

$$b_S(\omega_S, t) = b_S(\omega_S, T_{in}) e^{i\omega_S(T_{in}-t)} - i\sqrt{\frac{\gamma}{\pi}} \int_{T_{in}}^t \sigma_{\uparrow e}(t') e^{i\omega_S(t'-t)} dt' \quad (19)$$

If we assume that the atom-light interaction ends at time $T_{out} > t$, we have

$$b_J(\omega_J, t) = b_J(\omega_J, T_{out}) e^{i\omega_J(T_{out}-t)} - \sqrt{\frac{\kappa_J}{\pi}} \int_t^{T_{out}} a(t') e^{i\omega_J(t'-t)} dt' \quad (20)$$

$$b_S(\omega_S, t) = b_S(\omega_S, T_{out}) e^{i\omega_S(T_{out}-t)} + i\sqrt{\frac{\gamma}{\pi}} \int_t^{T_{out}} \sigma_{\uparrow e}(t') e^{i\omega_S(t'-t)} dt' \quad (21)$$

By integrating Eq. (18) with frequency, it is not difficult to obtain that

$$\sqrt{\frac{\kappa_J}{\pi}} \int_{-\infty}^{\infty} b_J(\omega_J, t) d\omega_J$$

$$= \sqrt{\frac{\kappa_J}{\pi}} \int_{-\infty}^{\infty} b_J(\omega_J, T_{in}) e^{i\omega_J(T_{in}-t)} d\omega_J$$

$$+ 2\kappa_J T_{in} t \int a(t') dt' \frac{1}{2\pi} \int_{-\infty}^{\infty} e^{i\omega_J(t'-t)} d\omega_J$$

$$= \sqrt{2\kappa_J} a_{J,in}(t) + \kappa_J a(t) \quad (22)$$

where we have used the relation[74]

$$\int_{t_0}^t f(t') \delta(t-t') dt' = \int_t^{t_1} f(t') \delta(t-t') dt' = \frac{1}{2} f(t), (t_0 < t < t_1), \quad (23)$$

and the assumptions ($J = R,T$)

$$a_{J,in}(t) = \frac{1}{\sqrt{2\pi}} \int_{-\infty}^{\infty} b_J(\omega_J, T_{in}) e^{i\omega_J(T_{in}-t)} d\omega_J \quad (24)$$

$$a_{J,out}(t) = \frac{1}{\sqrt{2\pi}} \int_{-\infty}^{\infty} b_J(\omega_J, T_{out}) e^{i\omega_J(T_{out}-t)} d\omega_J \quad (25)$$

$$a_{S,in}(t) = \frac{1}{\sqrt{2\pi}} \int_{-\infty}^{\infty} b_S(\omega_S, T_{in}) e^{i\omega_S(T_{in}-t)} d\omega_S \quad (26)$$

$$a_{S,out}(t) = \frac{1}{\sqrt{2\pi}} \int_{-\infty}^{\infty} b_S(\omega_S, T_{out}) e^{i\omega_S(T_{out}-t)} d\omega_S \quad (27)$$

Similarly, from Eqs. (19)–(21), we have

$$\sqrt{\frac{\gamma}{\pi}} \int_{-\infty}^{\infty} b_S(\omega_S, t) d\omega_S = \sqrt{2\gamma} a_{S,in}(t) - i\gamma\sigma_{\uparrow e}(t) \quad (28)$$

$$\sqrt{\frac{\kappa_J}{\pi}} \int_{-\infty}^{\infty} b_J(\omega_J, t) d\omega_J = \sqrt{2\kappa_J} a_{J,out}(t) - \kappa_J a(t) \quad (29)$$

$$\sqrt{\frac{\gamma}{\pi}} \int_{-\infty}^{\infty} b_S(\omega_S, t) d\omega_S = \sqrt{2\gamma} a_{S,out}(t) + i\gamma\sigma_{\uparrow e}(t) \quad (30)$$

Then, by substituting Eq. (22) and (29) into (13), we can obtain the dynamic equations

$$\frac{da(t)}{dt} = -i\omega_c a(t) - ig\sigma_{\uparrow e}(t) - \sqrt{2\kappa_R} a_{R,in}(t) - \kappa_R a(t) - \sqrt{2\kappa_T} a_{T,in}(t) - \kappa_T a(t) \quad (31)$$

$$\frac{da(t)}{dt} = -i\omega_c a(t) - ig\sigma_{\uparrow e}(t) - \sqrt{2\kappa_R} a_{R,out}(t) + \kappa_R a(t) - \sqrt{2\kappa_T} a_{T,in}(t) - \kappa_T a(t) \quad (32)$$

$$\frac{da(t)}{dt} = -i\omega_c a(t) - ig\sigma_{\uparrow e}(t) - \sqrt{2\kappa_R} a_{R,in}(t) - \kappa_R a(t) - \sqrt{2\kappa_T} a_{T,out}(t) + \kappa_T a(t) \quad (33)$$

By substituting Eq. (28, 30) into (14), we have

$$\frac{d}{dt}\sigma_{\uparrow e}(t) = -i\left(\omega_e - \omega_\uparrow\right)\sigma_{\uparrow e}(t) - iga(t) - i\sqrt{2\gamma} a_{S,in}(t) - \gamma\sigma_{\uparrow e}(t) \quad (34)$$

$$\frac{d}{dt}\sigma_{\uparrow e}(t) = -i\left(\omega_e - \omega_\uparrow\right)\sigma_{\uparrow e}(t) - iga(t) - i\sqrt{2\gamma} a_{S,out}(t) + \gamma\sigma_{\uparrow e}(t) \quad (35)$$

In the following, we assume that only the input on CM_R side is none-zero, i.e., $a_{T,in}(t) = a_{S,in}(t) = 0$. Then, by subtracting (31) and (32), we can get the relation between the input $a_{R,in}(t)$ and output $a_{R,out}(t)$,

$$a_{R,in}(t) + \sqrt{2\kappa_R} a(t) = a_{R,out}(t) \quad (36)$$

By subtracting (31) and (33), we have

$$a_{T,out}(t) = \sqrt{2\kappa_T} a(t) \quad (37)$$

By subtracting (34) and (35), we have

$$a_{S,out}(t) = -i\sqrt{2\gamma}\sigma_{\uparrow e}(t) \quad (38)$$

In addition to the above relations, we next calculate the steady-state solution of the dynamic Eq. (31, 32, 34) by assuming that the cavity-atom system is driven by the input light field with frequency ω. We suppose that

$$a_{R,in} = \alpha_{i,1\uparrow} e^{-i\omega t},$$

$$a(t) = \alpha e^{-i\omega t},$$

$$\sigma_{\uparrow e}(t) = \tilde{\sigma} e^{-i\omega t},$$

$$a_{R,out}(t) = \alpha_{R,1\uparrow} e^{-i\omega t},$$

$$a_{T,out}(t) = \alpha_{T,1\uparrow} e^{-i\omega t},$$

$$a_{S,out}(t) = \alpha_{S,1\uparrow} e^{-i\omega t} \quad (39)$$

Then, we can obtain that

$$\left[-\mathrm{i}(\omega_c - \omega) - \kappa_R - \kappa_T\right]\alpha - \mathrm{i}g\widetilde{\sigma} - \sqrt{2\kappa_R}\alpha_{i,1\uparrow} = 0 \tag{40}$$

$$\left[-\mathrm{i}(\omega_c - \omega) + \kappa_R - \kappa_T\right]\alpha - \mathrm{i}g\widetilde{\sigma} - \sqrt{2\kappa_R}\alpha_{R,1\uparrow} = 0 \tag{41}$$

$$\left[-\mathrm{i}(\omega_e - \omega_\uparrow - \omega) - \gamma\right]\widetilde{\sigma} - \mathrm{i}g\alpha = 0 \tag{42}$$

It is not difficult to get that

$$\alpha_{i,1\uparrow} = -\frac{\left[\mathrm{i}(\omega_c - \omega) + \kappa_R + \kappa_T\right]\left[\mathrm{i}(\omega_e - \omega_\uparrow - \omega) + \gamma\right] + g^2}{\sqrt{2\kappa_R}\left[\mathrm{i}(\omega_e - \omega_\uparrow - \omega) + \gamma\right]}\alpha \tag{43}$$

$$\alpha_{R,1\uparrow} = -\frac{\left[\mathrm{i}(\omega_c - \omega) - \kappa_R + \kappa_T\right]\left[\mathrm{i}(\omega_e - \omega_\uparrow - \omega) + \gamma\right] + g^2}{\sqrt{2\kappa_R}\left[\mathrm{i}(\omega_e - \omega_\uparrow - \omega) + \gamma\right]}\alpha \tag{44}$$

Equation (43) shows that when the input increases, the intensity of the cavity field also increase, resulting in the condition Eq. (15) not being satisfied.

With Eqs. (43) and (44), we can calculate Eq. (2). Suppose that the cavity and the external field are resonant, i.e., $\omega = \omega_c$, and $\Delta = \omega_e - \omega_\uparrow - \omega_c \equiv \omega_a - \omega_c$, we obtain

$$\frac{\alpha_{R,1\uparrow}}{\alpha_{i,1\uparrow}} = 1 - \frac{2\kappa_R(\mathrm{i}\Delta + \gamma)}{(\kappa_R + \kappa_T)(\mathrm{i}\Delta + \gamma) + g^2} \tag{45}$$

By using Eqs. (37) and (38), we can also have Eqs. (3) and (4), which are

$$\frac{\alpha_{T,1\uparrow}}{\alpha_{i,1\uparrow}} = -\frac{2\sqrt{\kappa_R \kappa_T}(\mathrm{i}\Delta + \gamma)}{(\kappa_R + \kappa_T)(\mathrm{i}\Delta + \gamma) + g^2} \tag{46}$$

$$\frac{\alpha_{S,1\uparrow}}{\alpha_{i,1\uparrow}} = \frac{2\sqrt{\kappa_R}\gamma g}{(\kappa_R + \kappa_T)(\mathrm{i}\Delta + \gamma) + g^2} \tag{47}$$

Cattiness calculation

Taking into account all possible light losses, the final state of the system after M cycles can be expressed as $|\psi_f\rangle = \frac{1}{\sqrt{2}}(|C_{0\uparrow}\rangle|\mathrm{loss}_\uparrow\rangle|\uparrow\rangle + |C_{0\downarrow}\rangle|\mathrm{loss}_\downarrow\rangle|\downarrow\rangle) = \frac{1}{\sqrt{2}}[\frac{1}{\sqrt{2}}(|\uparrow\rangle + |\downarrow\rangle)|\psi_0\rangle + \frac{1}{\sqrt{2}}(|\uparrow\rangle - |\downarrow\rangle)|\psi_1\rangle]$. After measuring the atom, the light field collapses to state $|\psi_{c=0,1}\rangle = \frac{1}{\sqrt{2}}(|C_{0\uparrow}\rangle|\mathrm{loss}_\uparrow\rangle + (-1)^c|C_{0\downarrow}\rangle|\mathrm{loss}_\downarrow\rangle)$ with equal probability. Its corresponding density matrix is denoted as $|\psi_c\rangle\langle\psi_c|$. By tracing over the loss terms, the resulting reduced dsensity matrix is obtained, represented as

$$\rho = Tr_{\mathrm{loss}}\{|\psi_c\rangle\langle\psi_c|\} = \frac{1}{2}|C_{0\uparrow}\rangle\langle C_{0\uparrow}| + \frac{1}{2}|C_{0\downarrow}\rangle\langle C_{0\downarrow}|$$

$$+(-1)^c\frac{1}{2}\langle\mathrm{loss}_\downarrow|\mathrm{loss}_\uparrow\rangle|C_{0\uparrow}\rangle\langle C_{0\downarrow}| + (-1)^c\frac{1}{2}\langle\mathrm{loss}_\uparrow|\mathrm{loss}_\downarrow\rangle|C_{0\downarrow}\rangle\langle C_{0\uparrow}| \tag{48}$$

By substituting ρ into the definition of cattiness[69–71]

$$C_a = -Tr[\rho \cdot L(\rho)] \tag{49}$$

with $L(\rho) = a\rho a^+ - \frac{1}{2}\rho a^+ a - \frac{1}{2}a^+ a\rho$, we can obtain that

$$C_a = -\sum_{\nu=0}^{\infty}\langle\nu|\rho a\rho a^+|\nu\rangle + \sum_{\nu=0}^{\infty}\nu\langle\nu|\rho^2|\nu\rangle \tag{50}$$

where $|\nu\rangle$ represents Fock state. Utilizing the following expressions ($j = \uparrow, \downarrow$),

$$\langle\nu|C_{0j}\rangle = \langle\nu|e^{-\frac{|C_{0j}|^2}{2}}\sum_{u=0}^{\infty}\frac{C_{0j}^u}{\sqrt{u!}}|u\rangle = e^{-\frac{|C_{0j}|^2}{2}}\frac{C_{0j}^\nu}{\sqrt{\nu!}} \tag{51}$$

we have

$$C_a = \frac{1}{4}\left(|\langle\mathrm{loss}_\uparrow|\mathrm{loss}_\downarrow\rangle|^2 - |\langle C_{0\uparrow}|C_{0\downarrow}\rangle|^2\right)|C_{0\uparrow} - C_{0\downarrow}|^2 \tag{52}$$

For comparison, we also give the expression for fidelity here, which is

$$F = \frac{1}{4}\left\{|\langle\alpha|C_{0\uparrow}\rangle|^2 + |\langle-\alpha|C_{0\downarrow}\rangle|^2 + 2\mathrm{Re}\left[\langle\alpha|C_{0\uparrow}\rangle\langle C_{0\downarrow}|-\alpha\rangle\langle\mathrm{loss}_\downarrow|\mathrm{loss}_\uparrow\rangle\right]\right\} \tag{53}$$

It can be easily seen that the fidelity is related to $|\langle\mathrm{loss}_\uparrow|\mathrm{loss}_\downarrow\rangle|$, while the cattiness is related to $|\langle\mathrm{loss}_\uparrow|\mathrm{loss}_\downarrow\rangle|^2$, and thus is more sensitive to light loss.

Data availability

All data generated or analyzed during the simulations of study are available from the corresponding author on reasonable request.

Code availability

The code employed to generate the simulations presented in this work is available upon request. Interested parties may inquire about access to the code by contacting the corresponding author.

References

1. Schrödinger, E. Die gegenwärtige situation in der Quantenmechanik. *Naturwissenschaften* **23**, 844 (1935).
2. Haroche, S. Nobel lecture: controlling photons in a box and exploring the quantum to classical boundary. *Rev. Mod. Phys.* **85**, 1083 (2013).
3. Wineland, D. J. Nobel lecture: superposition, entanglement, and raising Schrödinger's cat. *Rev. Mod. Phys.* **85**, 1103 (2013).
4. Sangouard, N. et al. Quantum repeaters with entangled coherent states. *J. Opt. Soc. Am. B* **27**, A137 (2010).
5. Brask, J. B., Rigas, I., Polzik, E. S., Andersen, U. L. & Sørensen, A. S. Hybrid long-distance entanglement distribution protocol. *Phys. Rev. Lett.* **105**, 160501 (2010).
6. Lee, S.-W. & Jeong, H. Near-deterministic quantum teleportation and resource-efficient quantum computation using linear optics and hybrid qubits. *Phys. Rev. A* **87**, 022326 (2013).
7. Jeong, H. & Kim, M. S. Efficient quantum computation using coherent states. *Phys. Rev. A* **65**, 042305 (2002).
8. Ralph, T. C., Gilchrist, A., Milburn, G. J., Munro, W. J. & Glancy, S. Quantum computation with optical coherent states. *Phys. Rev. A* **68**, 042319 (2003).
9. Lund, A. P., Ralph, T. C. & Haselgrove, H. L. Fault-tolerant linear optical quantum computing with small-amplitude coherent states. *Phys. Rev. Lett.* **100**, 030503 (2008).
10. Mirrahimi, M. et al. Dynamically protected cat-qubits: a new paradigm for universal quantum computation. *N. J. Phys.* **16**, 045014 (2014).
11. Su, D., Dhand, I. & Ralph, T. C. Universal quantum computation with optical four-component cat qubits. *Phys. Rev. A* **106**, 042614 (2022).

Article

12. Cochrane, P. T., Milburn, G. J. & Munro, W. J. Macroscopically distinct quantum-superposition states as a bosonic code for amplitude damping. *Phys. Rev. A* **59**, 2631 (1999).

13. Leghtas, Z. et al. Hardware-efficient autonomous quantum memory protection. *Phys. Rev. Lett.* **111**, 120501 (2013).

14. Bergmann, M. & van Loock, P. Quantum error correction against photon loss using multicomponent cat states. *Phys. Rev. A* **94**, 042332 (2016).

15. Ofek, N. et al. Extending the lifetime of a quantum bit with error correction in superconducting circuits. *Nature* **536**, 441 (2016).

16. Li, L. et al. Cat codes with optimal decoherence suppression for a lossy bosonic channel. *Phys. Rev. Lett.* **119**, 030502 (2017).

17. Hastrup, J. & Andersen, U. L. All-optical cat-code quantum error correction. *Phys. Rev. Res.* **4**, 043065 (2022).

18. Munro, W. J., Nemoto, K., Milburn, G. J. & Braunstein, S. L. Weak-force detection with superposed coherent states. *Phys. Rev. A* **66**, 023819 (2002).

19. Gilchrist, A. et al. Schrödinger cats and their power for quantum information processing. *J. Opt. B* **6**, S828 (2004).

20. Joo, J., Munro, W. J. & Spiller, T. P. Quantum metrology with entangled coherent states. *Phys. Rev. Lett.* **107**, 083601 (2011).

21. Zhang, Y. M., Li, X. W., Yang, W. & Jin, G. R. Quantum Fisher information of entangled coherent states in the presence of photon loss. *Phys. Rev. A* **88**, 043832 (2013).

22. Ghosh, S., Sharma, R., Roy, U. & Panigrahi, P. K. Mesoscopic quantum superposition of the generalized cat state: a diffraction limit. *Phys. Rev. A* **92**, 053819 (2015).

23. Facon, A. et al. A sensitive electrometer based on a Rydberg atom in a Schrödinger-cat state. *Nature* **535**, 262 (2016).

24. Polino, E., Valeri, M., Spagnolo, N. & Sciarrino, F. Photonic quantum metrology. *AVS Quant. Sci.* **2**, 024703 (2020).

25. Monroe, C., Meekhof, D. M., King, B. E. & Wineland, D. J. A "Schrödinger cat" superposition state of an atom. *Science* **272**, 1131 (1996).

26. Kienzler, D. et al. Observation of quantum interference between separated mechanical oscillator wave packets. *Phys. Rev. Lett.* **116**, 140402 (2016).

27. Deléglise, S. et al. Reconstruction of non-classical cavity field states with snapshots of their decoherence. *Nature* **455**, 510 (2008).

28. Vlastakis, B. et al. Deterministically encoding quantum information using 100-photon Schrödinger cat states. *Science* **342**, 607 (2013).

29. Neergaard-Nielsen, J. S., Nielsen, B. M., Hettich, C., Mølmer, K. & Polzik, E. S. Generation of a superposition of odd photon number states for quantum information networks. *Phys. Rev. Lett.* **97**, 083604 (2006).

30. Ourjoumtsev, A., Tualle-Brouri, R., Laurat, J. & Grangier, P. Generating optical Schrödinger kittens for quantum information processing. *Science* **312**, 83 (2006).

31. Gerrits, T. et al. Generation of optical coherent-state superpositions by number-resolved photon subtraction from the squeezed vacuum. *Phys. Rev. A* **82**, 031802 (2010).

32. Takahashi, H. et al. Generation of large-amplitude coherent-State superposition via ancilla-assisted photon subtraction. *Phys. Rev. Lett.* **101**, 233605 (2008).

33. Huang, K. et al. Optical synthesis of large-amplitude squeezed coherent-state superpositions with minimal resources. *Phys. Rev. Lett.* **115**, 023602 (2015).

34. Ourjoumtsev, A., Jeong, H., Tualle-Brouri, R. & Grangier, P. Generation of optical 'Schrödinger cats' from photon number states. *Nature* **448**, 784 (2007).

35. Ulanov, A. E., Fedorov, I. A., Sychev, D., Grangier, P. & Lvovsky, A. I. Loss-tolerant state engineering for quantum-enhanced metrology via the reverse Hong-Ou-Mandel effect. *Nat. Commun.* **7**, 11925 (2016).

36. Sychev, D. V. et al. Enlargement of optical Schrödinger's cat states. *Nat. Photon.* **11**, 379 (2017).

37. Hacker, B. et al. Deterministic creation of entangled atom–light Schrödinger-cat states. *Nat. Photon.* **13**, 110 (2019).

38. Dakna, M., Anhut, T., Opatrný, T., Knöll, L. & Welsch, D.-G. Generating Schrödinger-cat-like states by means of conditional measurements on a beam splitter. *Phys. Rev. A* **55**, 3184 (1997).

39. Takase, K., Yoshikawa, J.-i, Asavanant, W., Endo, M. & Furusawa, A. Generation of optical Schrödinger cat states by generalized photon subtraction. *Phys. Rev. A* **103**, 013710 (2021).

40. Lund, A. P., Jeong, H., Ralph, T. C. & Kim, M. S. Conditional production of superpositions of coherent states with inefficient photon detection. *Phys. Rev. A* **70**, 020101 (2004).

41. Laghaout, A. et al. Amplification of realistic Schrödinger-cat-state-like states by homodyne heralding. *Phys. Rev. A* **87**, 043826 (2013).

42. Wang, B. & Duan, L.-M. Engineering superpositions of coherent states in coherent optical pulses through cavity-assisted interaction. *Phys. Rev. A* **72**, 022320 (2005).

43. Reiserer, A., Ritter, S. & Rempe, G. Nondestructive detection of an optical photon. *Science* **342**, 1349 (2013).

44. Duan, L.-M. & Kimble, H. J. Scalable photonic quantum computation through cavity-assisted interactions. *Phys. Rev. Lett.* **92**, 127902 (2004).

45. Reiserer, A. & Rempe, G. Cavity-based quantum networks with single atoms and optical photons. *Rev. Mod. Phys.* **87**, 1379 (2015).

46. Mirrahimi, M. Cat-qubits for quantum computation. *C. R. Physique* **17**, 778 (2016).

47. Kwiat, P. G., Weinfurter, H., Herzog, T., Zeilinger, A. & Kasevich, M. A. Interaction-free measurement. *Phys. Rev. Lett.* **74**, 4763 (1995).

48. Salih, H., Li, Z.-H., Al-Amri, M. & Zubairy, M. S. Protocol for direct counterfactual quantum communication. *Phys. Rev. Lett.* **110**, 170502 (2013).

49. Li, Z.-H., Feng, S.-Y., Al-Amri, M. & Zubairy, M. S. Direct counterfactual quantum-communication protocol beyond a single-photon source. *Phys. Rev. A* **106**, 032610 (2022).

50. Wang, Z.-L. et al. A flying Schrödinger's cat in multipartite entangled states. *Sci. Adv.* **8**, eabn1778 (2022).

51. Bao, Z.-H. et al. Experimental preparation of generalized cat states for itinerant microwave photons. *Phys. Rev. A* **105**, 063717 (2022).

52. Ma, X.-S. et al. On-chip interaction-free measurements via the quantum Zeno effect. *Phys. Rev. A* **90**, 042109 (2014).

53. Cao, Y. et al. Direct counterfactual communication via quantum Zeno effect. *Proc. Natl. Acad. Sci.* **114**, 4920 (2017).

54. Liu, C., Liu, J.-H., Zhang, J.-X. & Zhu, S.-Y. The experimental demonstration of high efficiency interaction-free measurement for quantum counterfactual-like communication. *Sci. Rep.* **7**, 10875 (2017).

55. Liu, C., Yang, X.-F., Cui, L.-J., Zhou, S.-M. & Zhang, J.-X. Accurate measurement method for refractive index in a high efficiency interaction-free measurement system. *Opt. Express* **28**, 21916 (2020).

56. Li, Z.-H. et al. Counterfactual Trojan horse attack. *Phys. Rev. A* **101**, 022336 (2020).

57. Hance, J. R. & Rarity, J. Counterfactual ghost imaging. *npj Quant. Inform.* **7**, 88 (2021).

58. Scully, M. O. & Zubairy, M. S. *Quantum Optics* (Cambridge University Press, Cambridge, 1997).

59. Urban, E. et al. Observation of Rydberg blockade between two atoms. *Nat. Phys.* **5**, 110 (2009).

60. Johnson, T. A. et al. Rabi Oscillations between ground and Rydberg states with dipole-dipole atomic interactions. *Phys. Rev. Lett.* **100**, 113003 (2008).

61. Guo, Q., Cheng, L.-Y., Chen, L., Wang, H.-F. & Zhang, S. Counterfactual quantum-information transfer without transmitting any physical particles. *Sci. Rep.* **5**, 8416 (2015).

62. Birnbaum, K. M. et al. Photon blockade in an optical cavity with one trapped atom. *Nature* **436**, 87 (2005).

63. Nogues, G. et al. Seeing a single photon without destroying it. *Nature* **400**, 239 (1999).
64. Liu, Y. et al. Experimental demonstration of counterfactual quantum communication. *Phys. Rev. Lett.* **109**, 030501 (2012).
65. Kwiat, P. G. et al. High-efficiency quantum interrogation measurements via the quantum Zeno effect. *Phys. Rev. Lett.* **83**, 4725 (1999).
66. Bishop, A. I. & Barker, P. F. Subnanosecond pockels cell switching using avalanche transistors. *Rev. Sci. Instrum.* **77**, 044701 (2006).
67. Marinoni, A., Moeller, C. P., Rost, J. C., Porkolab, M. & Edlund, E. M. A pockels cell enabled heterodyne phase contrast imaging diagnostic for detection of ion cyclotron emission. *Rev. Sci. Instrum.* **93**, 083502 (2022).
68. Chen, N. et al. 1.9 μj external-cavity dumped ultra-broad-area semiconductor nanosecond laser. *Opt. Lett.* **48**, 3555 (2023).
69. Lee, C.-W. & Jeong, H. Quantification of macroscopic quantum superpositions within phase space. *Phys. Rev. Lett.* **106**, 220401 (2011).
70. Jeong, H., Kang, M. & Kwon, H. Characterizations and quantifications of macroscopic quantumness and its implementations using optical fields. *Opt. Commun.* **337**, 12 (2015).
71. Hacker, B. Two-photon gate and creation of optical cat states using one atom in a cavity, Ph.D. thesis, TU München (2019) https://mediatum.ub.tum.de/1485537.
72. Hu, C. Y., Young, A., O'Brien, J. L., Munro, W. J. & Rarity, J. G. Giant optical Faraday rotation induced by a single-electron spin in a quantum dot: applications to entangling remote spins via a single photon. *Phys. Rev. B* **78**, 085307 (2008).
73. Gardiner, C. W. & Collett, M. J. Input and output in damped quantum systems: quantum stochastic differential equations and the master equation. *Phys. Rev. A* **31**, 3761 (1985).
74. Walls, D. F. & Milburn, G. J. *Quantum Optics* (Springer- Verlag, Berlin, 1994).
75. Daiss, S. et al. A quantum-logic gate between distant quantum-network modules. *Science* **371**, 614 (2021).
76. Welte, S. et al. A nondestructive Bell-state measurement on two distant atomic qubits. *Nat. Photon.* **15**, 504 (2021).
77. Liu, Y. et al. Experimental twin-field quantum key distribution over 1000 km fiber distance. *Phys. Rev. Lett.* **130**, 210801 (2023).

Author contributions

Competing interests

The authors declare no competing interests.

Additional information

Supplementary information The online version contains supplementary material available at https://doi.org/10.1038/s42005-024-01617-6.

Correspondence and requests for materials should be addressed to Zheng-Hong Li, M. Al-Amri or M. Suhail Zubairy.

Peer review information *Communications Physics* thanks the anonymous reviewers for their contribution to the peer review of this work. A peer review file is available.

Reprints and permissions information is available at http://www.nature.com/reprints

Publisher's note Springer Nature remains neutral with regard to jurisdictional claims in published maps and institutional affiliations.